Deletion of rictor in brain and fat alters peripheral clock gene expression and increases blood pressure

Drägert, Katja ; Bhattacharya, Indranil ; Pellegrini, Giovanni ; Seebeck, Petra ; Azzi, Abdelhalim ; Brown, Steven A ; Georgiopoulou, Stavroula ; Held, Ulrike ; Blyszczuk, Przemyslaw ; Arras, Margarete ; Humar, Rok ; Hall, Michael N ; Battegay, Edouard ; Haas, Elvira

Abstract: The mammalian target of rapamycin complex 2 (mTORC2) contains the essential protein RICTOR and is activated by growth factors. mTORC2 in adipose tissue contributes to the regulation of glucose and lipid metabolism. In the perivascular adipose tissue, mTORC2 ensures normal vascular reactivity by controlling expression of inflammatory molecules. To assess whether RICTOR/mTORC2 contributes to blood pressure regulation, we applied a radiotelemetry approach in control and Rictor knockout (Rictor(aP2KO)) mice generated using adipocyte protein-2 gene promoter-driven CRE recombinase expression to delete Rictor. The 24-hour mean arterial pressure was increased in Rictor(aP2KO) mice, and the physiological decline in mean arterial pressure during the dark period was impaired. In parallel, heart rate and locomotor activity were elevated during the dark period with a pattern similar to blood pressure changes. This phenotype was associated with mild cardiomyocyte hypertrophy, decreased cardiac natriuretic peptides, and their receptor expression in adipocytes. Moreover, clock gene expression was reduced or phase-shifted in perivascular adipose tissue. No differences in clock gene expression were observed in the master clock suprachiasmatic nucleus, although Rictor gene expression was also lower in brain of Rictor(aP2KO) mice. Thus, this study highlights the importance of RICTOR/mTORC2 for interactions between vasculature, adipocytes, and brain to tune physiological outcomes, such as blood pressure and locomotor activity.

DOI: https://doi.org/10.1161/HYPERTENSIONAHA.115.05398

Deletion of *Rictor* in Brain and Fat Alters Peripheral Clock Gene Expression and Increases Blood Pressure

Katja Drägert, Indranil Bhattacharya, Giovanni Pellegrini, Petra Seebeck, Abdelhalim Azzi, Steven A. Brown, Stavroula Georgiopoulou, Ulrike Held, Przemyslaw Blyszczuk, Margarete Arras, Rok Humar, Michael N. Hall, Edouard Battegay, Elvira Haas

Abstract—The mammalian target of rapamycin complex 2 (mTORC2) contains the essential protein RICTOR and is activated by growth factors. mTORC2 in adipose tissue contributes to the regulation of glucose and lipid metabolism. In the perivascular adipose tissue, mTORC2 ensures normal vascular reactivity by controlling expression of inflammatory molecules. To assess whether RICTOR/mTORC2 contributes to blood pressure regulation, we applied a radiotelemetry approach in control and *Rictor* knockout (*Rictor*^{aP2KO}) mice generated using *adipocyte protein-2* gene promoter–driven CRE recombinase expression to delete *Rictor*. The 24-hour mean arterial pressure was increased in *Rictor*^{aP2KO} mice, and the physiological decline in mean arterial pressure during the dark period was impaired. In parallel, heart rate and locomotor activity were elevated during the dark period with a pattern similar to blood pressure changes. This phenotype was associated with mild cardiomyocyte hypertrophy, decreased cardiac natriuretic peptides, and their receptor expression in adipocytes. Moreover, clock gene expression was reduced or phase-shifted in perivascular adipose tissue. No differences in clock gene expression were observed in the master clock suprachiasmatic nucleus, although *Rictor* gene expression was also lower in brain of *Rictor*^{aP2KO} mice. Thus, this study highlights the importance of RICTOR/mTORC2 for interactions between vasculature, adipocytes, and brain to tune physiological outcomes, such as blood pressure and locomotor activity. **(*Hypertension*. 2015;66:00-00. DOI: 10.1161/HYPERTENSIONAHA.115.05398.)** ● **Online Data Supplement**

Key Words: adipose tissue ■ arterial pressure ■ circadian clocks ■ locomotor activity ■ mTOR complex 2 ■ RICTOR, mouse

The serine/threonine kinase mammalian target of rapamycin (mTOR) is ubiquitously expressed and exists in 2 multiprotein complexes, mTOR complex 1 (mTORC1) and complex 2 (mTORC2).[1,2] The rapamycin-insensitive companion of mTOR (RICTOR) is essential for the role of mTORC2 in propagating phosphoinositid-3-kinase elicited signals originating from hormones and growth factors.[2,3] mTORC2 phosphorylates and activates members of the AGC kinase family, such as AKT.[4] Adipocyte-specific ablation of *Rictor* results in higher lean mass because of increased levels of insulin and insulin-like growth factor -1, enhanced glucose metabolism, and insulin resistance in mice.[5,6] Using this mouse model, we have recently shown that vascular reactivity of the thoracic aorta with perivascular adipose tissue (PVAT) is altered and levels of inflammatory molecules in the PVAT are elevated.[7] However, the specificity of *adipocyte protein-2* (*aP2*) gene promoter–driven CRE recombinase expression for adipose tissue, an approach which was used for all above-mentioned studies, may vary and affect other tissues.[8] Consequently, target gene expression data from different organs should be considered for interpretation. In this study, we refer to these mice as *Rictor*^{aP2KO} mice.

In a healthy condition, PVAT releases vasoactive molecules conferring anticontractile properties to PVAT.[9] In obesity, PVAT's secretory profile changes to favor a proinflammatory state compromising PVAT's anticontractile properties.[10] Impaired PVAT function contributes to alterations in vascular reactivity which manifests itself in blood pressure changes as observed previously in a rat model of hypertension.[11] Intriguingly, inflammation is present in the vasculature in animal models of hypertension,[12,13] which supports the idea that inflammation of PVAT might play a significant role in the development of hypertension. The key characteristics

Received March 4, 2015; first decision March 18, 2015; revision accepted May 26, 2015.

From the Research Unit, Department of Internal Medicine (K.D., I.B., S.G., R.H, E.B., E.H.) and Division of Surgical Research (M.A.), University Hospital Zurich, Zurich, Switzerland; Center of Competence Multimorbidity and University Research Priority Program "Dynamics of Healthy Aging" (K.D., I.B., S.G., R.H, E.B., E.H.), Laboratory for Animal Model Pathology, Institute of Veterinary Pathology, Vetsuisse faculty (G.P.), Zurich Integrative Rodent Physiology (P.S.), Institute of Pharmacology and Toxicology (A.A., S.A.B.), Horten Center for Patient-Oriented Research and Knowledge Transfer (U.H.), Cardioimmunology, Center of Molecular Cardiology (P.B.), and Zurich Center for Integrative Human Physiology (E.B.), University of Zurich, Zurich, Switzerland; and Biozentrum, University of Basel, Basel, Switzerland (M.N.H.).

The online-only Data Supplement is available with this article at http://hyper.ahajournals.org/lookup/suppl/doi:10.1161/HYPERTENSIONAHA.115.05398/-/DC1.

Correspondence to Elvira Haas, Research Unit, Department of Internal Medicine, University Hospital Zurich, Wagistrasse 12, 8952 Schlieren, Zurich, Switzerland. E-mail Elvira.haas@usz.ch

of essential hypertension are hyperactivation of the renin–angiotensin aldosterone system and the sympathetic nervous system.[14] These 2 systems are also under the control of the circadian clock,[15] which is not surprising considering the diurnal fluctuations in blood pressure. Clock genes are part of a hierarchically organized circadian clock system in which the suprachiasmatic nucleus (SCN) in the hypothalamus serves as a master clock.[16] The SCN is entrained by the light/dark cycle and transmits humoral and neural signals to synchronize peripheral clocks located in most tissues, including the heart, adipose tissue, and blood vessels.[15]

In this study, we examined whether the increase in aortic contractility because of impaired PVAT function, which we reported previously, translates into elevated blood pressure.

Materials and Methods

Materials and Methods are available in the online-only Data Supplement.

Results

Mean Arterial Pressure Is Increased and Its Physiological Decline Nearly Absent in *Rictor*^{aP2KO} Mice

To investigate whether the increased aortic contractility which we observed previously in *Rictor*^{aP2KO} mice[7] translates into higher blood pressure, hemodynamic parameters were recorded using radiotelemetry. The 24-hour average of mean arterial pressure (MAP, Figure 1B, left panel; Table S1 in the online-only Data Supplement) and diastolic arterial pressure (Table S1) were increased in *Rictor*^{aP2KO} mice (+5.4 and +4.4 mm Hg, respectively; $P<0.05$), whereas systolic arterial pressure displayed an upward trend ($P=0.08$; Table S1) compared with control mice. Pulse pressure was similar between groups (Table S1). To determine diurnal patterns of MAP in *Rictor*^{aP2KO} and control mice, we analyzed data obtained from a telemetric measurement >7 days. Both groups displayed diurnal rhythmicity of MAP (Figure 1A, left panel). A detailed analysis for day 5 is shown in Figure 1A (right panel). However, the physiological decline of MAP in *Rictor*^{aP2KO} mice during the second half of the dark period appeared to be nearly absent (Figure 1A). Therefore, we analyzed MAP during the first and second half of the dark period separately. MAP was not significantly different during the first half of the dark period (Figure 1B, gray shaded area). Although decreasing significantly during the second half only in controls ($P<0.05$), MAP remained high in *Rictor*^{aP2KO} mice (Figure 1B, gray shaded area). The Pearson correlation coefficient between time and MAP values during the second half of the dark period for control and *Rictor*^{aP2KO} mice had median values of −0.3 and 0, respectively (Figure 1C). This suggests that the decline in MAP during the second half of the dark period is nearly absent in *Rictor*^{aP2KO} mice. In the first half of the light period, MAP values were different between groups ($P<0.05$), whereas MAP levels were similar in the second half, showing a steady increase with highest values at the transition to the dark period (Zeitgeber time [ZT]12/7:00 PM; Figure 1B). A detailed analysis of the diastolic arterial pressure, systolic arterial pressure, and heart rate (HR) for day 5 revealed that these blood pressure parameters followed similar patterns as MAP (Figure 1D).

Impaired Decline of Locomotor Activity During the Dark Period and Overall Hyperactivity in *Rictor*^{aP2KO} Mice

Locomotor activity is an important parameter that could account for the observed changes in blood pressure regulation.[17] In both mouse groups, the intensity of locomotor activity followed a diurnal pattern (Figure 2A). In control mice, locomotor activity peaked at the beginning of the dark period and gradually decreased as the dark period progressed. During the light period, only low activity was observed (Figure 2A, upper panel) in these mice. Interestingly, in the second half of the dark period, *Rictor*^{aP2KO} mice had a tendency to maintain high locomotor activity (Figure 2A, lower panel, grey shaded areas: 1:00 to 7:00 AM), which appeared to continue intermittently as indicated by the spikes during the light period (Figure 2A, lower panel). A detailed analysis for day 5 is shown in Figure 2B. Next, we quantified overall activity data collected during the telemetric measurements. During the light and dark periods, *Rictor*^{aP2KO} mice displayed a strong trend toward higher intensity of activity (light, $P=0.082$; dark, $P=0.18$; Table S2). Interestingly, the percentage of time during which mice show activity,[17] an alternative measure for locomotor activity, was increased in *Rictor*^{aP2KO} mice compared with controls during a 24-hour cycle (Figure 2D; Table S2). Analyzing the light and the dark periods separately, we observed a significant increase in the time during which *Rictor*^{aP2KO} mice show activity compared with controls (Table S2). During the dark period, this increase was remarkably more pronounced.

Differences in HR during the dark period amounted to +50 and +19 BPM during light period in *Rictor*^{aP2KO} mice compared with controls (Table S1; $P<0.05$). Similarly to MAP, HR remained high during the progression of the dark period (Figure S1). To visualize the similar patterns of MAP, HR, and locomotor activity during the dark period, these parameters were plotted in a single diagram displaying intensity of activity and MAP or HR, using 2 different *y*-axes (Figure S2A and S2B). The curves for the intensity of activity were highly similar to those for MAP and HR within the groups.

aP2 Promoter-Driven CRE Expression Ablates *Rictor* in Adipocytes and Brain

To confirm deletion of *Rictor* in adipocytes in our current set of *Rictor*^{aP2KO} mice, we measured mRNA expression levels in PVAT using quantitative real time–PCR. Steady-state mRNA expression levels of *Rictor* were reduced by 59% in PVAT, whereas they were similar in the aortic tissue between mouse groups (Figure 3A). As adipose tissue consists not only of adipocytes, but also other cells referred to as stromal vascular fraction, we separated adipocytes from stromal vascular fraction. In adipocytes from epididymal adipose tissue of *Rictor*^{aP2KO} mice, *Rictor* expression was decreased by 58%, whereas similar levels were measured in control and knockout stromal vascular fractions (Figure 3A). Further analysis of *Rictor* mRNA expression levels revealed no differences in the heart, kidney, liver, monocytes, and T cells between groups (Figure 3A). Interestingly, *Rictor*

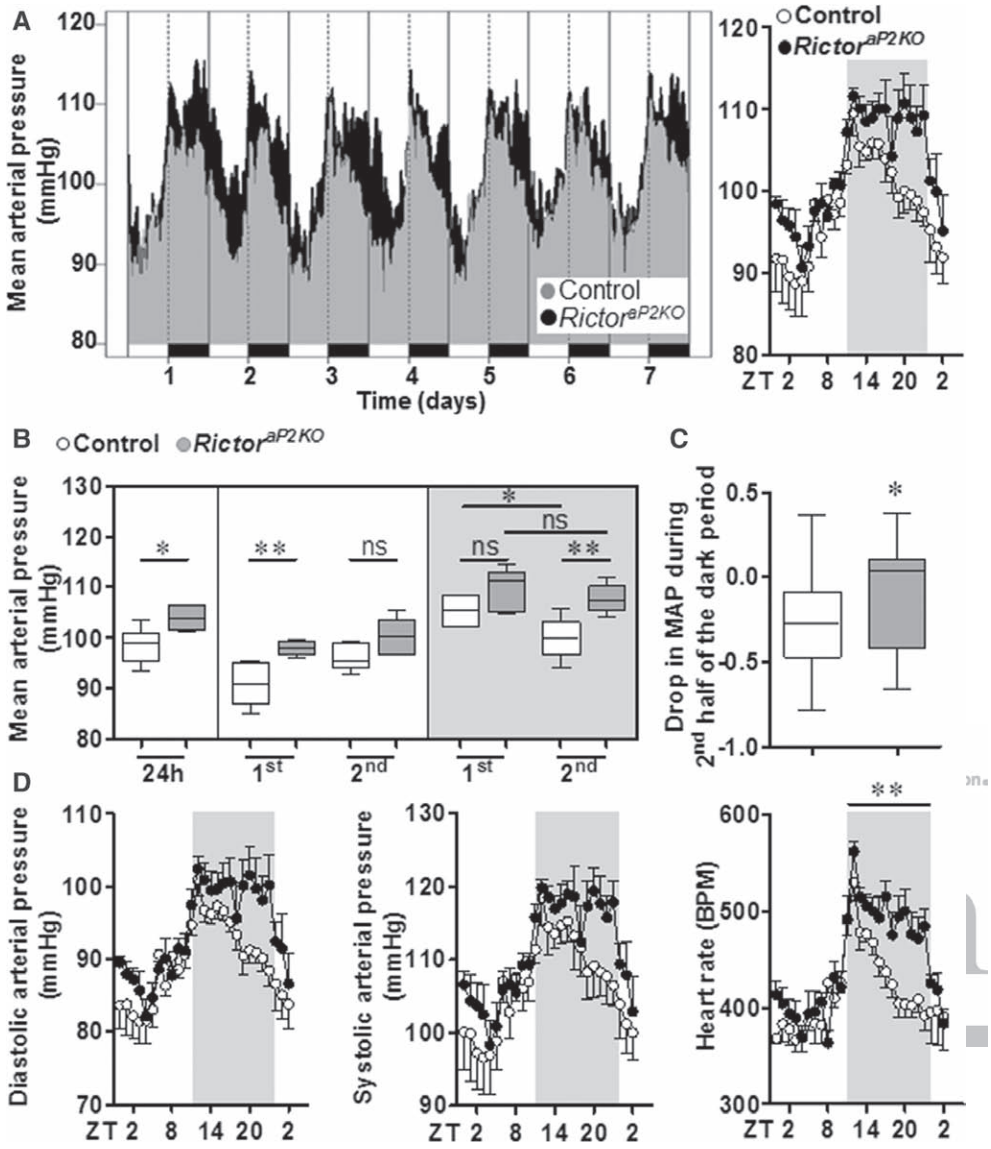

Figure 1. Mean arterial pressure (MAP) is increased and its physiological decline is strongly impaired in *Rictor* knockout (*Rictor*^{aP2KO}) mice. **A** (**left**), Diurnal fluctuations of MAP are represented as 1 hour running median in *Rictor*^{aP2KO} and control mice. The 12:12 hour light/dark cycle is schematically depicted as white and black bars, respectively (light was switched on at Zeitgeber time (ZT) 0: 7:00 AM; light off: 7:00 PM/ZT12). **A** (**right**), MAP values are represented as hourly means±SEM on day 5. The gray shaded area denotes the dark period. **B**, MAP measurements were analyzed during 24 hours, for the first and second half of the light and dark periods, separately. The median is indicated as a horizontal line. **C**, MAP drops in control, but not in *Rictor*^{aP2KO} mice during the second half relative to the first half of the dark period. **D**, Diastolic and systolic arterial pressure and heart rate were analyzed in the conditions outlined in **A**. n=5/6. **P*<0.05 and ***P*<0.01 vs control; ns indicates nonsignificant.

mRNA levels were decreased in the brain (SCN by 76%; cortex by 66%, Figure 3A). Collectively, these data suggest that *Rictor* is specifically ablated in the adipocytes and brain, whereas stromal vascular fraction and aortic tissue were not affected.

We further characterized the impact of *Rictor* deletion in PVAT and brain. Histological examination of cross-sections of thoracic aortas with PVAT revealed higher perivascular cell density in *Rictor*^{aP2KO} mice compared with controls (Figure 3B, right panel). Consistently, the number of nuclei was 57% higher in PVAT from *Rictor*^{aP2KO} mice (*P*<0.01; Figure 3B). Brains of *Rictor*^{aP2KO} mice appeared smaller (Figure 3C, left panel), and absolute brain weight was decreased by 17% compared with controls (Figure 3C, right panel).

Evidence of Mild Cardiomyocyte Hypertrophy in *Rictor*^{aP2KO} Mice

Next, we performed morphological assessment of the heart to evaluate the presence of possible hypertrophic changes. Mean absolute heart weights were higher in *Rictor*^{aP2KO} mice (Figure 4A), whereas mean relative to body heart weights were not changed compared with controls (Figure 4A). Right ventricular free wall and interventricular septal thickness were increased in *Rictor*^{aP2KO} mice (*P*=0.09 and *P*=0.08, respectively, Figure 4A). The hearts of *Rictor*^{aP2KO} mice exhibited histological changes consistent with mild cardiomyocyte hypertrophy, as indicated by a 25% increase in the cardiomyocyte cross-sectional area (Figure 4B, *P*<0.01). Staining

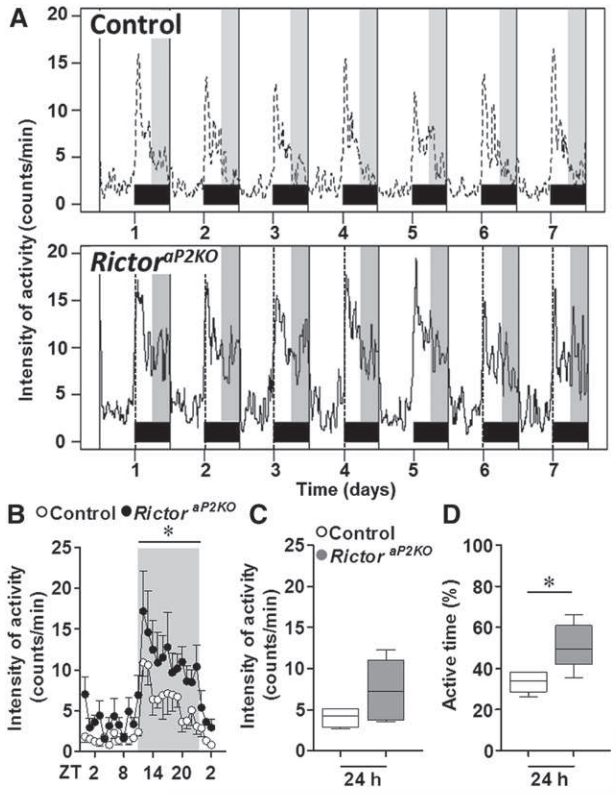

Figure 2. Intensity of activity and active time are increased in *Rictor* knockout (*Rictor*^{aP2KO}) mice. **A**, Values plotted represent the 1 hour running median of the intensity of activity for control and *Rictor*^{aP2KO} mice. The black bars at the **bottom** indicate the 12 hour dark period and the grey shaded areas correspond to the second half of the dark period in *Rictor*^{aP2KO} and control, respectively. **B**, Locomotor activity measurements were analyzed during 24 hour on day 5. The gray shaded area indicates the dark period. Values are means±SEM. **C**, Intensity of activity and (**D**) active time during a 24-hour cycle are represented. The median for each group is indicated as a horizontal line. n=5/6. **P*<0.05 vs control.

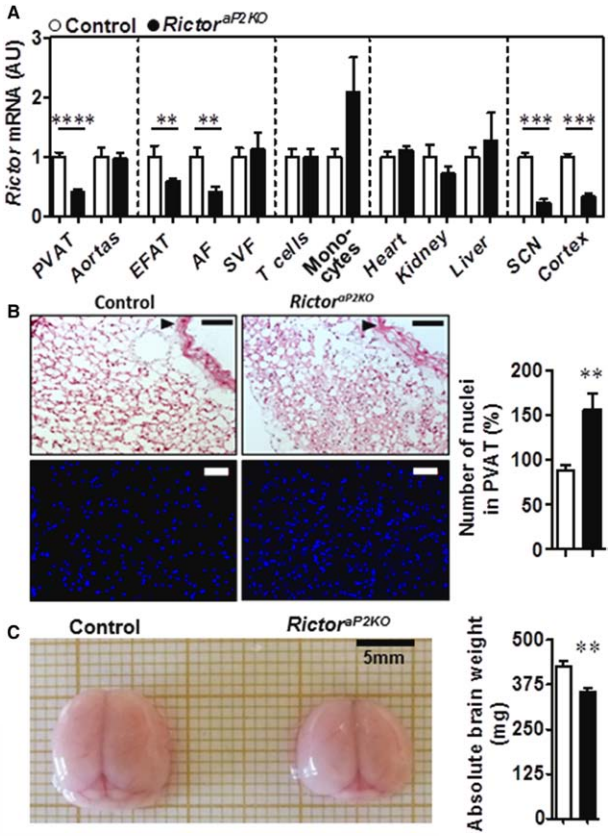

Figure 3. *aP2*/CRE-driven deletion of *Rictor* decreases expression of *Rictor* in adipocytes and brain. **A**, Steady-state mRNA expression levels of *Rictor* were determined using quantitative RT-PCR in *Rictor* knockout (*Rictor*^{aP2KO}) and control mice. Values are expressed in arbitrary units (AU). Perivascular adipose tissue (PVAT): n=8, aortas: n=7/8, epididymal adipose tissue (EFAT): n=8/9, adipocyte fraction (AF): n=7/11, stromal vascular fraction (SVF): n=4, T cells and monocytes: n=2/4, heart and kidney: n=7/8, liver: n=3, suprachiasmatic nucleus (SCN): n=3/5, and cortex: n=3/5. **B**, Cross-sections of thoracic aortas with PVAT from control and *Rictor*^{aP2KO} mice stained with hematoxylin/eosin (**upper**, black bar: 100 μm), and Hoechst (**lower**, white bar: 50 μm). Arrowheads indicate the thoracic aorta. Cell density of the perivascular tissue was determined by counting Hoechst-stained nuclei (n=5). **C**, Representative photographs of brains and quantification of absolute brain weight from each genotype (n=7/8). Values are means±SEM. ***P*<0.01, ****P*<0.005, and *****P*<0.001 vs control.

with Masson's trichrome revealed no evidence of fibrosis in the myocardium (data not shown). As it has been shown that *Rictor*^{aP2KO} mice exhibit increased organ size,[5] we suspect that increased absolute heart weights and mild enlargement of the cardiomyofibres are most likely because of the overall phenotype, rather than to a compensatory change secondary to the only mild increase in blood pressure. In addition, there were no findings consistent with vascular remodeling secondary to hypertension,[18] such as narrowing of the lumen, medial hypertrophy or increased adventitial fibrosis in the aorta or in the renal and pulmonary small and large arteries of *Rictor*^{aP2KO} mice (Figure S3 and data not shown). Representative cross-sections of heart, kidney, and aortic arch are shown in Figure S3. Interestingly, gene expression levels of cardiac hypertrophy biomarkers were decreased in the heart of *Rictor*^{aP2KO} mice: atrial natriuretic peptide (NP) was decreased by 52% (P<0.05), whereas brain NP and β-myosin heavy chain showed a strong downwards trend (Figure 4C, left panel). The NPs bind to the transmembrane high affinity NP receptors NPR1, NPR2, and NPR3.[19] These receptors are expressed in adipocytes to regulate adipose tissue metabolism, including lipolysis and adipokine secretion.[19] *Npr2* and *Npr3* mRNA expression levels were decreased in adipocytes isolated from epididymal adipose tissue by 51% and 45%, respectively (Figure 4C, middle panel). A similar expression pattern of NP receptors was measured in PVAT (Figure 4C, right panel). In contrast, the *Anp* gene expression was nearly absent in PVAT.

Higher Insulin Levels and Variations in *Rictor*^{aP2KO} Mice

In previous studies using *aP2* gene promoter–driven CRE recombinase to knockout *Rictor* in mice,[5,6] diurnal fluctuations of insulin were not investigated. Therefore, we measured insulin levels every 4 hours during a 24-hour cycle (Figure S4A). Insulin levels were higher at the beginning of the light period at ZT2 (9:00 AM), and a trend toward higher insulin levels could also be observed during the dark period at ZT14 (9:00 PM) and ZT18 (1:00 AM; Figure S4A). Overall, levels of insulin varied 7.6-fold during a 24-hour cycle, whereas in controls only a 1.6-fold variation was quantified (Figure S4A).

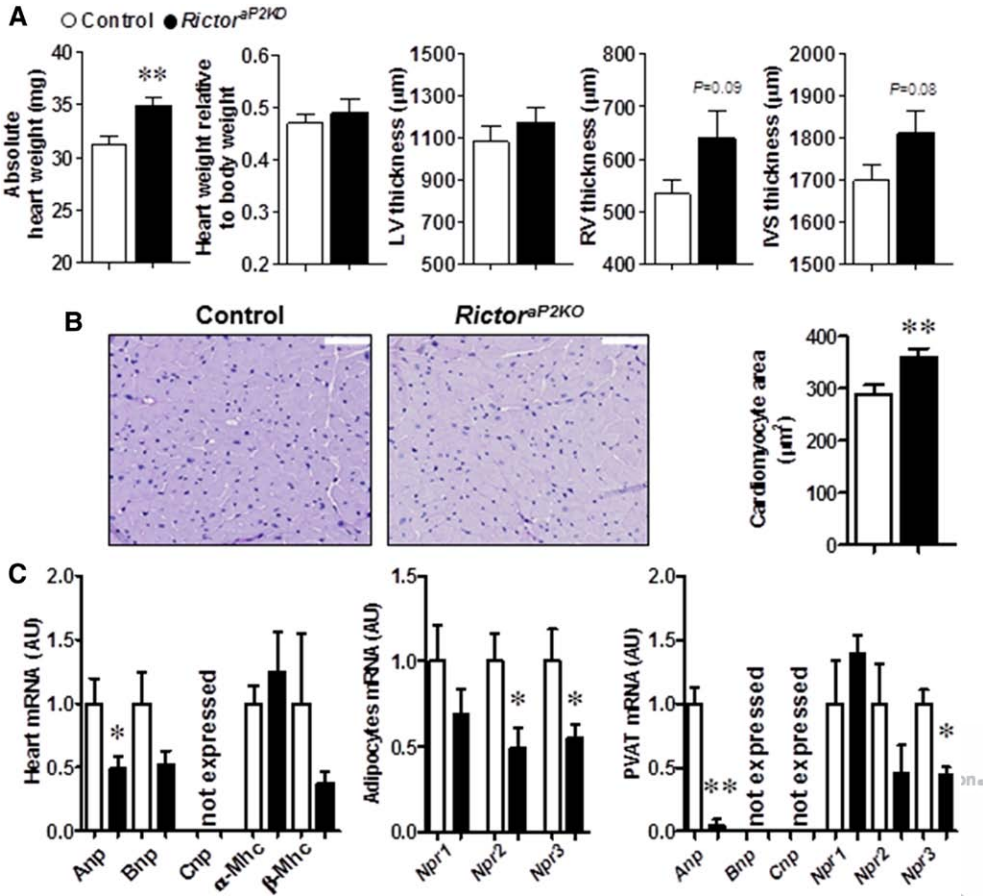

Figure 4. Mild cardiomyocyte hypertrophy and decreased gene expression of natriuretic peptides and their receptors in *Rictor* knockout (*Rictor*^{aP2KO}) mice. **A**, Quantification of total heart weight, heart weight relative to body weight, left ventricle (LV), right ventricle (RV), and interventricular septum (IVS) thickness, n=7/8. **B**, Representative images of heart tissue stained with Periodic acid–Schiff reaction (white bar: 50 µm) and quantification of cardiomyocyte area. **C**, Steady-state mRNA expression levels of indicated genes were determined in heart (**left**, n=7/8), in adipocytes from epididymal adipose tissue (**middle**, n=6/7), and in perivascular adipose tissue (PVAT; **right**, n=3) using quantitative RT-PCR. Values are expressed in arbitrary units (AU). **P*<0.05 and ***P*<0.01 vs control. Anp indicates atrial natriuretic peptide; Bnp, brain natriuretic peptide; Cnp, C-type natriuretic peptide; Mhc, myosin heavy chain; and Npr, natriuretic peptide receptor.

Glucose levels in serum were significantly higher at the end of the light period (ZT10; 5:00 PM) followed by a sharp decline at ZT14 in *Rictor*^{aP2KO} mice, indicating that higher insulin levels might lead to decreased glucose plasma levels at the beginning of the dark period. (Figure S4B).

Identification of Differentially Expressed Genes in PVAT of *Rictor*^{aP2KO} Mice

Data from blood pressure and locomotor activity analyses revealed a complex phenotype in the *Rictor*^{aP2KO} mice which could not be explained solely by the induction of proinflammatory molecule expression in PVAT. To identify differentially expressed genes in PVAT of *Rictor*^{aP2KO} mice, we performed a microarray analysis. Gene Ontology analysis of differentially expressed genes (Table S4) revealed the circadian rhythm as the most affected pathway in PVAT (Table S3). The data have been deposited in GEO database (Accession Number: GSE67077).

Divergent Clock Gene Expression in PVAT, But Not in the Suprachiasmatic Nucleus, in *Rictor*^{aP2KO} Mice

To further examine the impact of *Rictor* deletion on clock genes, we analyzed mRNA expression levels of core clock genes *Bmal1, Clock, Npas2, Cry1/2, Per1/2*, *Rev-Erb-alpha* (*Rev-Erb-*α), and *Ror*α during a 24-hour cycle in PVAT and in aortic tissue (Figure 5 and Figure S5, respectively). In aortic tissue, mRNA expression levels were mostly comparable between mouse groups and followed similar diurnal patterns (Figure S5). In PVAT, expression of *Clock*, *Cry1*, *Per1*, and *Ror*α was lower only during the light period in *Rictor*^{aP2KO} mice compared with controls (Figure 5). For *Per2*, a phase-shift at the transition from the light to the dark periods was observed. Collectively, these data suggest that ablation of *Rictor* in adipocytes strongly affects clock gene expression in PVAT, but has only minimal effects on these genes in the aortic tissue. We found that the circadian rhythm of blood pressure (Figure 1) and locomotor activity (Figure 2) is altered in *Rictor*^{aP2KO} mice. Thus, we quantified clock gene expression in the SCN during a 24-hour cycle. No differences in the mRNA expression levels of *Bmal1*, *Npas2*, *Clock*, *Cry1/2*, *Per1/2*, *Rev-Erb-*α, and *Ror*α were detected between mouse groups (Figure 6). Collectively, these findings indicate that decreased *Rictor* expression in the SCN does not affect core clock gene expression, whereas expressional changes of *Clock*, *Ror*α, *Per1*/2, and *Cry1* in PVAT are likely to contribute to increased blood pressure observed in *Rictor*^{aP2KO} mice.

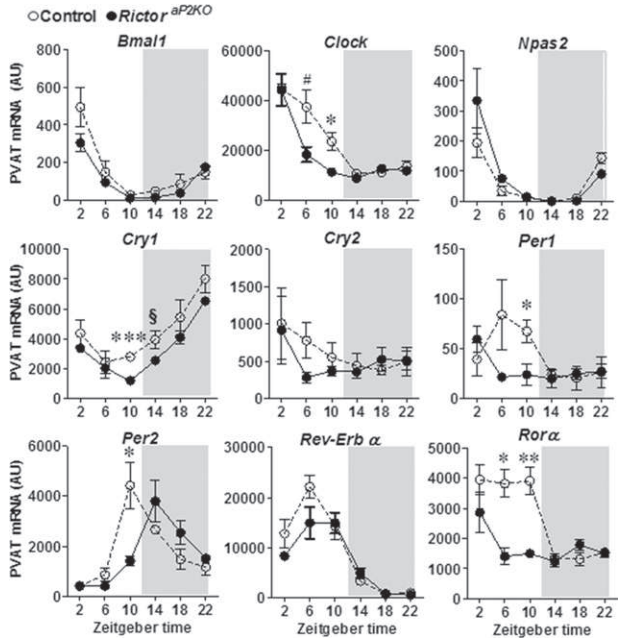

Figure 5. Steady-state mRNA expression levels of core clock genes are different in perivascular adipose tissue (PVAT) from *Rictor* knockout (*Rictor*^{aP2KO}) mice during the light period. mRNA expression levels of core clock genes in PVAT were determined using quantitative RT-PCR. Gray shaded areas represent the 12 hour dark period. Values are expressed in arbitrary units (AU). n=3 per group and time point. **P*<0.05, ***P*<0.01, ****P*<0.005, #*P*=0.06, and §*P*=0.08 vs control.

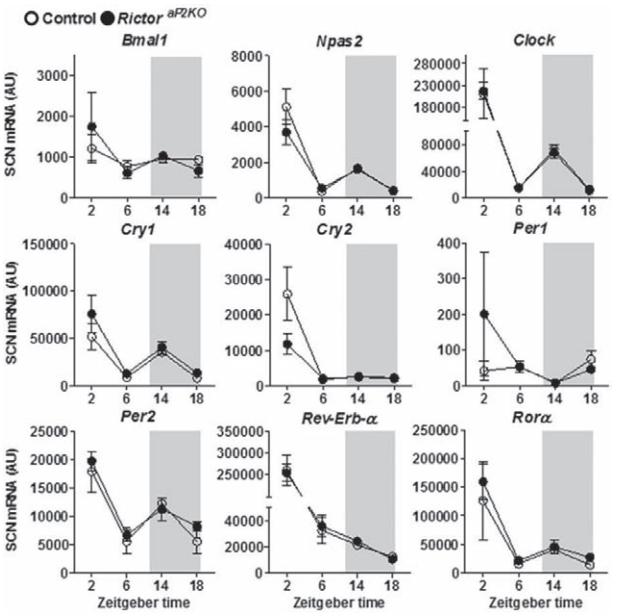

Figure 6. Deletion of *Rictor* does not affect core clock gene expression in the suprachiasmatic nucleus. mRNA expression levels of core clock genes in the suprachiasmatic nucleus (SCN) of *Rictor* knockout (*Rictor*^{aP2KO}) and control mice were analyzed using quantitative RT-PCR. Gray shaded areas represent the 12 hour dark period. Values are expressed in arbitrary units (AU). n=3/5 per group and time point.

Discussion

This is the first study to show that RICTOR/mTORC2 acts as a regulator for coordinated diurnal expression of clock genes in PVAT, but not in the SCN. At the whole body level, RICTOR/mTORC2 in adipose and brain tissue contributes to the diurnal regulation of blood pressure and locomotor activity. The presented data demonstrate the importance of the mTORC2 signaling pathway in the brain to adipocyte axis for daily fluctuations of physiological processes.

We and others have recently shown that mTORC2 activity controls inflammatory molecule expression using tissue-specific *Rictor* knockout mouse models.[7,20] We showed that vascular contractility in *Rictor*^{aP2KO} mice is increased because of enhanced secretion of proinflammatory cytokines in PVAT.[7] Ablation of *Rictor* strongly reduced AKT^{Ser473} phosphorylation, resulting in impaired mTORC2 signaling.[5–7] Consequently, we assign the observed changes in *Rictor*^{aP2KO} mice to the impaired mTORC2 downstream signaling.

In this study, we explored these findings further by studying blood pressure regulation in *Rictor*^{aP2KO} mice. In line with our hypothesis, *Rictor*^{aP2KO} mice showed increased MAP and alterations of its diurnal patterns. The increase in blood pressure parameters was too small to be considered as hypertension. In fact, our observations rather point toward a phenotype in *Rictor*^{aP2KO} mice which is termed prehypertension in patients.[21] The term prehypertension is defined as blood pressure levels of 120 to 139 mm Hg for systolic and 80 to 89 mm Hg for diastolic blood pressure, respectively.[21] Applying this definition to mice, we established a prehypertensive phenotype in the *Rictor*^{aP2KO} mice. At the tissue level, we found that cell density of thoracic PVAT, shown to be highly similar to brown adipose tissue,[22] is increased in *Rictor*^{aP2KO} mice. Intriguingly, it has been demonstrated that perivascular cell density is increased in an animal model of hypertension,[11] and that adipocytes in brown adipose tissue lacking *Rictor* are smaller.[23] This led us to speculate that elevated blood pressure is at least partially linked to the higher cell density in PVAT of *Rictor*^{aP2KO} mice.

NPs are hormonal regulators of vasodilation and natriuresis lowering blood pressure.[24] We report that *Anp* and *Bnp* mRNA expression levels are reduced in hearts of *Rictor*^{aP2KO} mice. Our results obtained in mice are in agreement with the findings in a study with patients showing that a prehypertensive state is associated with a deficiency of circulating brain NP levels.[25] Interestingly, low plasma levels of NPs have been identified as a common predisposition for metabolic and cardiovascular diseases.[19] In line with data from hyperinsulinemic rats displaying a hypertensive phenotype,[26] we showed that in *Rictor*^{aP2KO} mice hyperinsulinemia is associated with increased HR and blood pressure. Thus, high levels of insulin and its strong variability during the course of the day might disable appropriate diurnal blood pressure regulation and reduce expression of *Anp* and *Bnp* in *Rictor*^{aP2KO} mice. Studying other pathophysiological mechanisms of hypertension,[27] such as the activation of the renin–angiotensin aldosterone system and the sympathetic nervous system, and changes in salt sensitivity was beyond the scope of this study. Particularly, the possible impact of angiotensin II on the regulation of insulin-dependent AKT activation warrants further investigation because angiotensin II plays a major role in the pathogenesis of insulin resistance and in the

diurnal regulation of blood pressure.[28] We focused on locomotor activity, another important factor that can influence HR and blood pressure.[17] Locomotor activity was sustained and high in *Rictor*^{aP2KO} mice during the dark period, which could explain in part the strong impairment of the physiological decline of MAP in *Rictor*^{aP2KO} mice.

We also investigated the deletion of *Rictor* in different organs in more detail, based on the fact that the tissue specificity of the *aP2* gene promoter used to produce the conditional knockout may not be restricted to adipocytes.[8,29] Interestingly, activity of the *aP2* promoter–driven CRE recombinase in the brain was established[8,29] and confirmed by our data. Using the brain-specific nestin promoter to drive CRE expression in floxed *Rictor* mice, Thomanetz et al[30] demonstrated that brain size was reduced by about 40% compared with controls. We found a 17% reduction in brain size in *Rictor*^{aP2KO} mice, indicating that different approaches to target *Rictor* in the brain may result in brain size reduction of variable magnitude.[30] The current approach to knockout *Rictor* resulted in a 50% to 75% reduction of *Rictor* gene expression in adipose tissues and brain. Therefore, we considered a potential impact of *Rictor* deletion in the brain, particularly in the SCN where the biological master clock is located to alternatively explain the observed changes in daily rhythmicity of blood pressure and locomotor activity in *Rictor*^{aP2KO} mice. Tightly regulated clock genes control daytime-dependent behaviors and mammalian physiology.[31] Mutations and deletions of clock genes in mice have been associated with changes in blood pressure and its diurnal patterns.[32] In the SCN, diurnal expression of core clock genes remained unaltered during the 24-hour cycle. These results imply that changes in blood pressure and locomotor activity observed in *Rictor*^{aP2KO} mice are regulated downstream or independently of the molecular clock mechanism in the SCN. Thus, the present data underpin the importance of the exact tuning of *Rictor* expression in the brain–adipose axis to ensure daily oscillation of physiological processes. The impact of *Rictor* deletion in other brain regions possibly influencing the observed phenotype of *Rictor*^{aP2KO} mice needs further investigation.

In contrast, genome-wide mRNA expression analysis revealed a significant impact of *Rictor* deletion on peripheral clock gene expression in PVAT. Further analysis during a 24-hour cycle revealed significantly reduced expression of clock genes *Rorα*, *Per1*, *Cry1,* and *Clock* and *Per2* phase-shift in PVAT of *Rictor*^{aP2KO} mice. Interestingly, *Rorα* and *Per1/Per2* have been shown to contribute to the regulation of inflammatory processes in the cardiovascular system[33] and in the adipose tissue.[34] Decreased expression of *Per1*/2, *Cry1,* and *Clock* was shown in inflamed epididymal adipose tissue of genetically obese *ob/ob* mice.[34] Thus, reduced *Rorα*, *Per1*, *Cry1*, and *Clock* gene expression might facilitate the proinflammatory molecule expression in *Rictor*^{aP2KO} mice which we observed previously[7] and increase in blood pressure.

Perspectives

In summary, this study establishes the importance of RICTOR/mTORC2 in the regulation of the interactions between vasculature, adipocytes, and brain to tune oscillatory physiological outcomes, such as blood pressure and locomotion. These interactions are likely to be mediated by hormones, such as insulin and NPs. Further experiments are needed to elucidate these complex relationships which might give hints for effective strategies to combat prehypertensive conditions in patients.

Acknowledgments

Special thanks go to Dr Jelena Kühn-Georgijevic and Dr Hubert Rehrauer from Functional Genomic Center Zurich for their support with microarray and data analysis. We would like to thank Nadine Naegele from the Institute of Physiology (University of Zurich) for performing glucose analysis in blood serum. We are grateful to all members of research unit, Internal Medicine, University Hospital Zurich for stimulating discussions and, in addition, to Ana Perez-Dominguez for her excellent technical assistance.

Sources of Funding

This work was supported by funding from University of Zurich, University Hospital of Zurich, Hartmann Müller Stiftung, Forschungskredit of the University of Zurich (Grant-No. FK-13–026), the Swiss National Science Foundation (Grant No. 118349), Stiftung Baugarten, and Jubiläumsstiftung der Schweizerischen Lebensversicherungs- und Rentenanstalt für Volksgesundheit und medizinische Forschung (Swiss Life).

Disclosures

None.

References

1. Laplante M, Sabatini DM. mTOR signaling in growth control and disease. *Cell*. 2012;149:274–293. doi: 10.1016/j.cell.2012.03.017.
2. Wullschleger S, Loewith R, Hall MN. TOR signaling in growth and metabolism. *Cell*. 2006;124:471–484. doi: 10.1016/j.cell.2006.01.016.
3. Laplante M, Sabatini DM. An emerging role of mTOR in lipid biosynthesis. *Curr Biol*. 2009;19:R1046–R1052. doi: 10.1016/j.cub.2009.09.058.
4. Oh WJ, Jacinto E. mTOR complex 2 signaling and functions. *Cell Cycle*. 2011;10:2305–2316.
5. Cybulski N, Polak P, Auwerx J, Rüegg MA, Hall MN. mTOR complex 2 in adipose tissue negatively controls whole-body growth. *Proc Natl Acad Sci U S A*. 2009;106:9902–9907. doi: 10.1073/pnas.0811321106.
6. Kumar A, Lawrence JC Jr, Jung DY, Ko HJ, Keller SR, Kim JK, Magnuson MA, Harris TE. Fat cell-specific ablation of rictor in mice impairs insulin-regulated fat cell and whole-body glucose and lipid metabolism. *Diabetes*. 2010;59:1397–1406. doi: 10.2337/db09-1061.
7. Bhattacharya I, Drägert K, Albert V, Contassot E, Damjanovic M, Hagiwara A, Zimmerli L, Humar R, Hall MN, Battegay EJ, Haas E. Rictor in perivascular adipose tissue controls vascular function by regulating inflammatory molecule expression. *Arterioscler Thromb Vasc Biol*. 2013;33:2105–2111. doi: 10.1161/ATVBAHA.112.301001.
8. Lee KY, Russell SJ, Ussar S, Boucher J, Vernochet C, Mori MA, Smyth G, Rourk M, Cederquist C, Rosen ED, Kahn BB, Kahn CR. Lessons on conditional gene targeting in mouse adipose tissue. *Diabetes*. 2013;62:864–874. doi: 10.2337/db12-1089.
9. Brown NK, Zhou Z, Zhang J, Zeng R, Wu J, Eitzman DT, Chen YE, Chang L. Perivascular adipose tissue in vascular function and disease: a review of current research and animal models. *Arterioscler Thromb Vasc Biol*. 2014;34:1621–1630. doi: 10.1161/ATVBAHA.114.303029.
10. Van de Voorde J, Boydens C, Pauwels B, Decaluwe K. Perivascular adipose tissue, inflammation and vascular dysfunction in obesity. *Curr Vasc Pharmacol*. 2014;12:403–411.
11. Li R, Andersen I, Aleke J, Golubinskaya V, Gustafsson H, Nilsson H. Reduced anti-contractile effect of perivascular adipose tissue on mesenteric small arteries from spontaneously hypertensive rats: role of Kv7 channels. *Eur J Pharmacol*. 2013;698:310–315. doi: 10.1016/j.ejphar.2012.09.026.
12. Savoia C, Schiffrin EL. Inflammation in hypertension. *Curr Opin Nephrol Hypertens*. 2006;15:152–158. doi: 10.1097/01.mnh.0000203189.57513.76.
13. Harrison DG, Guzik TJ, Lob HE, Madhur MS, Marvar PJ, Thabet SR, Vinh A, Weyand CM. Inflammation, immunity, and hypertension.

Hypertension. 2011;57:132–140. doi: 10.1161/HYPERTENSIONAHA.110.163576.
14. Takahashi H, Yoshika M, Komiyama Y, Nishimura M. The central mechanism underlying hypertension: a review of the roles of sodium ions, epithelial sodium channels, the renin-angiotensin-aldosterone system, oxidative stress and endogenous digitalis in the brain. *Hypertens Res*. 2011;34:1147–1160. doi: 10.1038/hr.2011.105.
15. Dibner C, Schibler U, Albrecht U. The mammalian circadian timing system: organization and coordination of central and peripheral clocks. *Annu Rev Physiol*. 2010;72:517–549. doi: 10.1146/annurev-physiol-021909-135821.
16. Kohsaka A, Waki H, Cui H, Gouraud SS, Maeda M. Integration of metabolic and cardiovascular diurnal rhythms by circadian clock. *Endocr J*. 2012;59:447–456.
17. Van Vliet BN, McGuire J, Chafe L, Leonard A, Joshi A, Montani JP. Phenotyping the level of blood pressure by telemetry in mice. *Clin Exp Pharmacol Physiol*. 2006;33:1007–1015. doi: 10.1111/j.1440-1681.2006.04479.x.
18. Intengan HD, Schiffrin EL. Vascular remodeling in hypertension: roles of apoptosis, inflammation, and fibrosis. *Hypertension*. 2001;38(3 Pt 2):581–587.
19. Gruden G, Landi A, Bruno G. Natriuretic peptides, heart, and adipose tissue: new findings and future developments for diabetes research. *Diabetes Care*. 2014;37:2899–2908. doi: 10.2337/dc14-0669.
20. Festuccia WT, Pouliot P, Bakan I, Sabatini DM, Laplante M. Myeloid-specific Rictor deletion induces M1 macrophage polarization and potentiates *in vivo* pro-inflammatory response to lipopolysaccharide. *PLoS One*. 2014;9:e95432. doi: 10.1371/journal.pone.0095432.
21. Chobanian AV, Bakris GL, Black HR, Cushman WC, Green LA, Izzo JL Jr, Jones DW, Materson BJ, Oparil S, Wright JT Jr, Roccella EJ; National Heart, Lung, and Blood Institute Joint National Committee on Prevention, Detection, Evaluation, and Treatment of High Blood Pressure; National High Blood Pressure Education Program Coordinating Committee. The Seventh Report of the Joint National Committee on Prevention, Detection, Evaluation, and Treatment of High Blood Pressure: the JNC 7 report. *JAMA*. 2003;289:2560–2572. doi: 10.1001/jama.289.19.2560.
22. Fitzgibbons TP, Kogan S, Aouadi M, Hendricks GM, Straubhaar J, Czech MP. Similarity of mouse perivascular and brown adipose tissues and their resistance to diet-induced inflammation. *Am J Physiol Heart Circ Physiol*. 2011;301:H1425–H1437. doi: 10.1152/ajpheart.00376.2011.
23. Hung CM, Calejman CM, Sanchez-Gurmaches J, Li H, Clish CB, Hettmer S, Wagers AJ, Guertin DA. Rictor/mTORC2 loss in the Myf5 lineage reprograms brown fat metabolism and protects mice against obesity and metabolic disease. *Cell Rep*. 2014;8:256–271. doi: 10.1016/j.celrep.2014.06.007.
24. Gardner DG, Chen S, Glenn DJ, Grigsby CL. Molecular biology of the natriuretic peptide system: implications for physiology and hypertension. *Hypertension*. 2007;49:419–426. doi: 10.1161/01.HYP.0000258532.07418.fa.
25. Macheret F, Heublein D, Costello-Boerrigter LC, Boerrigter G, McKie P, Bellavia D, Mangiafico S, Ikeda Y, Bailey K, Scott CG, Sandberg S, Chen HH, Malatino L, Redfield MM, Rodeheffer R, Burnett J, Jr, Cataliotti A. Human hypertension is characterized by a lack of activation of the antihypertensive cardiac hormones ANP and BNP. *J Am Coll Cardiol*. 2012;60:1558–1565. doi: 10.1016/j.jacc.2012.05.049.
26. Kuo JJ, Jones OB, Hall JE. Chronic cardiovascular and renal actions of leptin during hyperinsulinemia. *Am J Physiol Regul Integr Comp Physiol*. 2003;284:R1037–R1042. doi: 10.1152/ajpregu.00480.2002.
27. Oparil S, Zaman MA, Calhoun DA. Pathogenesis of hypertension. *Ann Intern Med*. 2003;139:761–776.
28. Sueta D, Koibuchi N, Hasegawa Y, Toyama K, Uekawa K, Katayama T, Ma M, Nakagawa T, Waki H, Maeda M, Ogawa H, Kim-Mitsuyama S. Blood pressure variability, impaired autonomic function and vascular senescence in aged spontaneously hypertensive rats are ameliorated by angiotensin blockade. *Atherosclerosis*. 2014;236:101–107. doi: 10.1016/j.atherosclerosis.2014.06.016.
29. Martens K, Bottelbergs A, Baes M. Ectopic recombination in the central and peripheral nervous system by aP2/FABP4-Cre mice: implications for metabolism research. *FEBS Lett*. 2010;584:1054–1058. doi: 10.1016/j.febslet.2010.01.061.
30. Thomanetz V, Angliker N, Cloëtta D, Lustenberger RM, Schweighauser M, Oliveri F, Suzuki N, Rüegg MA. Ablation of the mTORC2 component rictor in brain or Purkinje cells affects size and neuron morphology. *J Cell Biol*. 2013;201:293–308. doi: 10.1083/jcb.201205030.
31. Brown SA, Azzi A. Peripheral circadian oscillators in mammals. *Handb Exp Pharmacol*. 2013:45–66.
32. Rudic RD, Fulton DJ. Pressed for time: the circadian clock and hypertension. *J Appl Physiol (1985)*. 2009;107:1328–1338. doi: 10.1152/japplphysiol.00661.2009.
33. Duez H, Staels B. The nuclear receptors Rev-erbs and RORs integrate circadian rhythms and metabolism. *Diab Vasc Dis Res*. 2008;5:82–88. doi: 10.3132/dvdr.2008.0014.
34. Yamaoka M, Maeda N, Takayama Y, Sekimoto R, Tsushima Y, Matsuda K, Mori T, Inoue K, Nishizawa H, Tominaga M, Funahashi T, Shimomura I. Adipose hypothermia in obesity and its association with period homolog 1, insulin sensitivity, and inflammation in fat. *PLoS One*. 2014;9:e112813. doi: 10.1371/journal.pone.0112813.

Novelty and Significance

What Is New?

- RICTOR in adipose tissue and brain contributes to the regulation of blood pressure and locomotion.
- RICTOR stabilizes diurnal fluctuations of clock gene expression and affects cell density in perivascular adipose tissue, but has no impact on clock genes in the suprachiasmatic nucleus.
- Gene expression of natriuretic peptides and their receptors is reduced in the heart and adipocytes of *Rictor*^{aP2K0} mice.

What Is Relevant?

- Reduced *Rictor* expression may be a key event during prehypertension in patients facilitating progression of the disease by increasing perivascular adipose tissue inflammation and by dampening of the protective signaling of natriuretic peptides.
- RICTOR in the brain–adipocyte axis contributes to the regulation of fluctuating physiological functions, such as blood pressure and locomotion.

Summary

At the tissue level, *aP2* gene promoter–driven CRE recombinase expression to ablate *Rictor* gene expression results in a higher cell density and impaired daily fluctuations of core clock genes in perivascular adipose tissue.

At the whole body level, RICTOR/mTORC2 in adipose tissue and brain modulates diurnal fluctuations in blood pressure and locomotion and results in a smaller brain. The underlying mechanism possibly involves impaired perivascular adipose tissue function, induction of hyperinsulinemia, and reduced natriuretic peptide signaling.

ONLINE SUPPLEMENT

DELETION OF RICTOR IN BRAIN AND FAT ALTERS PERIPHERAL CLOCK GENE EXPRESSION AND INCREASES BLOOD PRESSURE

Katja Drägert[1,2], Indranil Bhattacharya[1,2], Giovanni Pellegrini[3], Petra Seebeck[4], Abdelhalim Azzi[5], Steven A. Brown[5], Stavroula Georgiopoulou[1,2], Ulrike Held[6], Przemyslaw Blyszczuk [7], Margarete Arras[8], Rok Humar[1,2], Michael N. Hall[9], Edouard Battegay[1,2,10], Elvira Haas[1,2]

[1]Research Unit, Department of Internal Medicine, University Hospital Zurich

[2]Center of Competence Multimorbidity and University Research Priority Program "Dynamics of Healthy Aging", University of Zurich

[3]Institute of Veterinary Pathology, Vetsuisse Faculty, University of Zurich

[4]Zurich Integrative Rodent Physiology, University of Zurich

[5]Institute of Pharmacology and Toxicology, University of Zurich

[6]Horten Center for Patient-Oriented Research and Knowledge Transfer, University of Zurich

[7] Cardioimmunology, Center of Molecular Cardiology, University of Zurich

[8]Division of Surgical Research, University Hospital Zurich, Switzerland

[9]Biozentrum, University of Basel

[10]Zurich Center for Integrative Human Physiology, University of Zurich

All Switzerland

Correspondence to: Elvira Haas, Research Unit, Department of Internal Medicine, University Hospital Zurich, Wagistrasse 12, 8952 Schlieren, Switzerland
Email: Elvira.haas@usz.ch, Phone: +41 44 5563234, Fax: +41 44 5563232

1. Methods

Mice and tissue collection

Mice used in the present study were described in detail before [1]. Briefly, mice with deletion of *Rictor* (*Rictor*^{aP2KO}) were generated by crossing *Rictor*$^{fl/fl}$ mice with C57BL/6J mice expressing CRE recombinase under the control of the *adipocyte protein 2* (*aP2,* also known as fatty acid binding protein 4*)* gene promoter (purchased from JAX Laboratories, Bar Harbor, Maine, USA). In all experiments, male mice (18-23 weeks old) were used and as control group, littermates without the *Cre* transgene (*Rictor*$^{fl/fl}$, termed henceforth control).

Mice were kept in the institutional animal facilities (University of Zurich and University Hospital of Zurich, Switzerland) at 22 °C with a 12:12 hour light/dark cycle. Light onset was at 7 am [zeitgeber time (ZT) 0] and light offset was at 7 pm (ZT 12). Animals had access to standard chow (4.5 % calories from fat; Kliba Nafag, Kaiseraugust, Switzerland) and water *ad libitum*. All mice used were genotyped for *Rictor* (standard PCR) and *Cre* recombinase (quantitative RT-PCR) using specific mouse primers (Table S5) and standard protocols (JAX Laboratories, Bar Harbor, Maine, USA). Before sacrifice, mice were weighed and anesthetized by intraperetoneal (i.p.) injection (xylazine: 20; ketamine: 100; and acepromazine: 3.0; in mg/kg body weight) and exsanguinated via cardiac puncture. Mice used for confirmation of the *Rictor* knockout in PVAT and aortas (aortic tissue) and for the genome expression study were starved overnight and sacrificed at 9 am.

All mouse experiments described here were approved by the Kantonales Veterinaeramt of Zurich, Switzerland (License numbers ZH44/2011 and ZH184/2014). Therewith, the investigation conforms to the Guide for the Care and Use of Laboratory Animals published by the US National Institutes of Health (8th Edition, 2011).

Isolation of T cells and monocytes using fluorescence activated cell sorting

Freshly isolated spleens were passed through 70 µm and 40 µm cell strainers in order to obtain single cell suspension. Erythrocytes were depleted by 2 minute incubation in ACK buffer. Cells were incubated with the appropriate combination of fluorochrome-conjugated antibodies: anti-CD4 (clone RM4-4), anti-CD11c (N418, both eBioscience), anti-I-A/I-E (2G9, BD Bioscience), anti-CD11b (M1/70), anti-CD3 (17A2), and anti-Ly6C (HK1.4, all Biolegend). $CD3^+CD4^+$ splenocytes were identified as $CD4^+$ T lymphocytes cells and $CD11b^+CD11c^-$MHC-II^-Ly-$6C^{hi}$ splenocytes as inflammatory monocytes. Propidium iodide (PI, eBioscience) was used to exclude dead cells. Cells were sorted with FACSAria III (BD Bioscience).

Tissue collection and histological analysis

For analysis of tissues during a 24 hour period, 3 mice from each group were sacrificed every 4 hours and different tissues from control and *Rictor*^{aP2KO} mice were collected. The first mouse groups were sacrificed at 9 am (ZT 2), 2 hours after light onset. For tissue collection during the dark period, mice were euthanized under red light to ensure no disruption of the 12:12 hour light/dark cycle. Mice were not starved before sacrifice.

After euthanasia, body weights were collected at necropsy to allow calculation of organ to body weight ratios. A complete necropsy, including a thorough external and internal gross post mortem examination was performed on each mouse. Heart and brain from each mouse were excised, dried on filter paper and weighed. Mouse heart weights were normalized to body weights (HW/BoW). Representative samples of all organs and tissues were harvested and fixed in 10 % neutral buffered formalin.

PVAT was dissected from the thoracic aorta and aortic arch and tissues were immediately placed in RNA*later*™ (Qiagen, Hilden, Germany) or directly snap-frozen. Blood collected in ethylenediamine tetraacetic acid (EDTA) tubes during exsanguination was centrifuged at 8000 x g for 15 min at 4 °C, plasma in the supernatant snap-frozen and kept with all the other collected tissues at -80 °C until further analysis.

After routine paraffin wax embedding, sections (3-5 µm) were prepared and stained with haematoxylin and eosin (HE). Histological analysis was performed on the heart, aortic arch, lungs and kidneys. Three cross sections were obtained from each heart at standard distances from the apex, to visualize the left and right ventricles. The Masson's Trichrome stain was applied for the visualization of collagen fibers in the heart and lungs [2]. All slides were scanned using digital slide scanner NanoZoomer-XR C12000 (Hamamatsu, Japan) and images were taken using NDP.view2 viewing software (Hamamatsu, Japan). Cross sectional lengths of the septal wall and right and left ventricular free walls were measured.

Cardiomyocyte cross-sectional area was employed as index of cardiac hypertrophy. Periodic acid-Schiff (PAS) staining on 3-5 µm heart sections was applied to better outline the cardiomyocyte boundaries and quantify cardiomyocyte cross-sectional area. Scanned slide images were taken as mentioned above. In all mice, measurements were taken from the outline of 50 randomly selected cardiomyocytes exhibiting a clear cross-cut nucleus. Measurements were done using ImageJ 1.48 software (http://imagej.nih.gov/ij/index.html).

Recording of blood pressure and locomotor activity in mice using radiofrequency transmitters

Control and *Rictor*^{aP2KO} mice (n=5-6 per group) were implanted with a telemetry sender (TA11PA-C10, Data Sciences International, St. Paul, MN, USA) via the left carotid artery to monitor simultaneously mean (MAP), diastolic (DAP) and systolic arterial pressure (SAP), pulse pressure, heart rate (HR), and locomotor activity. Operation and post-operative care procedures were described previously [3]. Briefly, mice were anesthetized with isoflurane, and the telemetry sender implanted in the left carotid artery. The transmitter, connected with the telemetry sender via a small catheter, was positioned under the skin between the right front and hind limb. Mice were kept warm on a heating pad and monitored until fully recovered from anesthesia. After surgery, mice were single caged in a warming cabinet at 30 °C in a 12:12 hour light/dark cycle with access to food and water *ad libitum*. Recovery from surgery was allowed for 7 days before measurements were started. During measurement, mice were housed individually and the temperature in the warming cabinet was adjusted to 25 °C. Blood pressure and locomotor activity data were determined from day 8 after surgery during the following week up to three weeks post telemetry sender implantation. Data from each telemetry sender were transmitted to a receiver plate (RPC-1, Data Sciences International, St. Paul, USA) positioned

below each cage and thereafter collected using the Dataquest A.R.T. system, version 4.2 (Data Sciences International, St. Paul, USA). Blood pressure was measured for 30 seconds every 5 minutes. Locomotor activity was recorded continuously by the frequency of movement of each animal across the cage in counts/min (intensity of activity). For analysis of locomotor activity, less than 0.6 counts per minute were considered as inactive and set to 0 for further calculations.

RNA isolation, reverse transcription and quantitative real-time PCR

RNA from PVAT, EFAT and adipocytes was extracted using RNeasy® lipid tissue kit, from thoracic aortas, and heart using RNeasy® fibrous tissue kit, from kidney, liver and stromal vascular fraction using RNeasy® mini kit, and T cells and monocytes using RNeasy® plus mini kit according to the protocol of the manufacturer (Qiagen, Hombrechtikon, Switzerland) respectively, including an on-column DNase digestion (RNase-free DNase, Qiagen). Before reverse transcription, RNA quantity and quality was determined using Nanodrop 2000 Spectrophotometer and Agilent 2100 Bioanalyzer. Reverse transcription of 50 ng RNA from PVAT, stromal vascular fraction and thoracic aortas was performed using WT (Whole Transcript)-Ovation® Pico RNA Amplification System (Nugen, Bemmel, Netherlands) and from EFAT, adipocytes, heart, kidney, liver, T cells and monocytes using iScript™ Reverse Transcription Supermix according manufactures recommendations (BioRad, Hercules, CA, USA). For quantitative RT-PCR, final cDNA concentration was adjusted to 10 ng in a 15 µl reaction volume. Each reaction was performed in duplicates using Bio-Rad CFX96 Real-Time System and iQ™ SYBR® Green Supermix (BioRad, Hercules, CA, USA) and specific mouse primers. Gene expression in PVAT, thoracic aortas, EFAT and adipocytes was normalized to the reference gene *acidic ribosomal phosphoprotein* (*Arbp*), in heart, kidney and liver to the reference gene *cyclophelin B* and in the stromal vascular fraction to the reference gene *TATA box binding protein* (*Tbp*) using the comparative C(T) method [4]. If not otherwise noted, mouse primer pairs for selected genes were designed using Primer Blast (NCBI, USA) [5] and are listed in supplementary method **Table S4**.

Isolation of RNA from suprachiasmatic nucleus and brain cortex

The brain was dissected, placed in artificial cerebrospinal fluid (ACSF; NaCl - 120 mM; KCl - 2.5 mM; $MgCl_2$ x 6*H_2O - 1 mM; NaH_2PO_4 x 2*H_2O; - 1.25 mM; $NaHCO_3$ - 26 mM; HEPES - 5 mM; $CaCl_2$ - 2 mM; glucose - 16 mM; pH 7.35) and 250 to 300 µm brain slices were cut using a vibratom (Leica VT 1200, Leica Biosystems, Switzerland). Brain regions containing the SCN and cortex were identified under a binocular (Olympus SZ61, Volketswil, Switzerland), cut out, and stored at - 80°C until further analysis. SCN and cortex were homogenized in 300 µl RLT-buffer with β-mercaptoethanol by vortexing the samples 3 x 10 sec at room temperature. RNA was extracted using RNeasy® micro kit according the recommendations of the manufacturer (Qiagen, Hombrechtikon, Switzerland). 5 µl eluat from the isolation columns were reversed transcribed to cDNA using WT (Whole Transcript)-Ovation Pico RNA Amplification System (Nugen, Bemmel, Netherlands). cDNA transcription and quantitative RT-PCR were performed as described above and relative gene expression levels were normalized to *glyceraldehyde-3-phosphate dehydrogenase* (*Gapdh*).

Bioplex analysis

Bioplex assay was performed using blood plasma collected from control and *Rictor*^{aP2KO} mice. Concentrations of insulin were measured using corresponding components of BioPlex™ Pro Mouse Diabetes assay according to the manufacturer's protocol in a Bioplex™ 100 machine (BioRad, Hercules CA, USA). Data were analyzed using BioPlex™ Manager 4.1.1 software and quantified based on the Logistic-5PL regression standard curve.

Glucose levels in blood plasma

Plasma glucose levels were determined in *Rictor*^{aP2KO} and control mice using UniCel DxC 800 System and specific reagent, calibration and control kits for glucose measurement (Beckman Coulter, Galway, Ireland) according to the manufacturer's recommendations.

Histology of thoracic aorta and PVAT

10 µm cross sections from thoracic aortas with PVAT were cut as described previously [6]. Prior to staining, slides were dried for 20 min at room temperature, fixed in 4 % PFA in PBS (pH 7.4) for 10 minutes and washed twice for 5 min in aqua-dest. Haematoxylin staining was performed using Mayer's haematoxylin (Dako, Baar, Switzerland) for 3-5 min followed by a 5 min washing step under slowly running tap water. For differentiation, slides were dunk twice in acidic alcohol (0.3 % HCl in 70 % EtOH) and washed immediately in aqua dest. For eosin staining, slides were incubated 30 sec in 0.1 % Eosin (Sigma, Buchs, Switzerland) washed immediately in deionized water and differentiated in 70 % Ethanol for 3 sec. Slides were washed twice for 2 min in deionized water and air dried. Coverslips were mounted with Eukit quick-hardening mounting medium (Sigma, Buchs, Switzerland) onto slides.
Staining of the nuclei using Hoechst: Fixed cross-sections were incubated for 60 min with blocking buffer (5 % goat serum in PBS / 0.1 % TWEEN). Slides were washed twice for 5 min with PBS (pH 7.4) and nuclei were stained with Hoechst (2 µg/µL in PBS, pH 7.4, Life Technologies) for 5 min. Slides were washed 3 x 5 min with PBS (pH 7.4) and mounted with fluorescent mounting medium (Dako, Baar, Switzerland).
Slides were dried at least 1 day before imaging. Images were acquired using CLSM Leica SP5 microscope and LAS-AF 2.6.3.8173 software (Leica, Heerbrugg, Switzerland). Nuclei were counted using image J 1.48 for Windows (NIH, USA) in a 475 x 340 µm area.

Whole-genome expression study

Total RNA was isolated from PVAT surrounding the thoracic part of the arterial tree from control and *Rictor*^{aP2KO} mice. Total RNA was extracted using the RNeasy® lipid tissue kit according manufacturer's recommendation (Qiagen, Hombrechtikon, Switzerland). DNase digestion of isolated total RNA was performed in solution (RNase-free DNase, Qiagen), followed by an additional purification step of total RNA using RNeasy® mini kit according manufactures protocol (Qiagen, Hombrechtikon, Switzerland). Before further analysis, RNA quality and quantity was determined using

Nanodrop 2000 Spectrophotometer and Agilent 2100 Bioanalyzer. Only total RNA with an RNA integrity number (RIN) > 8 were considered for further analysis.

Total RNA was reverse transcribed and cDNA amplified using Ambion® WT Expression kit (Affymetrix, United Kingdom) following manufacturer's protocols. Biotinylated cDNA was prepared using Encore Biotine Module (Nugen, Netherlands) according to manufacturer's recommendations and hybridized to Affymetrix Mouse Gene® 1.0 ST array strips (Affymetrix, Santa Clara, CA). Gene Chips were scanned using the Hewlett-Packard GeneArray Scanner G2500A (Hewlett-Packard, Böblingen, Germany) and expression data analysed with Affymetrix Power Tools v1.10.2 (Affymetrix, Santa Clara, CA) using the RMA algorithm. The data discussed in this publication have been deposited in NCBI's Gene Expression Omnibus [7] and are accessible through GEO Series accession number GSE67077 (http://www.ncbi.nlm.nih.gov/geo/query/acc.cgi?&acc=GSE67077).

For further data analysis, genes were considered to be differentially expressed in *Rictor*^{aP2KO} mice if $P<0.05$ and fold change > 1.5. A gene ontology analysis was performed with genes identified using GeneGo Analysis program (www.genego.com).

Statistical analysis

Data are expressed as means ± standard error of the mean (SEM) or as box blots in which the median is represented by a horizontal line. To this end, data from each mouse were compiled to one data point (mean) and are represented in box blots according to the mouse groups. Comparisons between groups for other experiments were analyzed by two-tailed Student's t-test. For displaying MAP, levels of locomotor activity and heart rate over time, we used running medians to smooth data. Differences were considered statistically significant at values of $P<0.05$. Statistical analyses were performed using GraphPad Prism 5.04 program for Windows (GraphPad software, SanDiego, CA, USA) and R for Windows (R Core Team 2014). R: A language and environment for statistical computing (R Foundation for Statistical Computing, Vienna, Austria. URL http://www.R-project.org/).

2. References

1. Cybulski N, Polak P, Auwerx J, Ruegg MA, Hall MN. Mtor complex 2 in adipose tissue negatively controls whole-body growth. *Proc Natl Acad Sci U S A*. 2009;106:9902-9907.

2. Luna L. Manual of histologic staining methods of the armed forces institute of pathology. *McGraw-Hill, NY*. 1968;3rd edition:94-95.

3. Schuler B, Rettich A, Vogel J, Gassmann M, Arras M. Optimized surgical techniques and postoperative care improve survival rates and permit accurate telemetric recording in exercising mice. *BMC veterinary research*. 2009;5:28.

4. Schmittgen TD, Livak KJ. Analyzing real-time pcr data by the comparative c(t) method. *Nat Protoc*. 2008;3:1101-1108.

5. Ye J, Coulouris G, Zaretskaya I, Cutcutache I, Rozen S, Madden TL. Primer-blast: A tool to design target-specific primers for polymerase chain reaction. *BMC bioinformatics*. 2012;13:134.

6. Bhattacharya I, Dragert K, Albert V, Contassot E, Damjanovic M, Hagiwara A, Zimmerli L, Humar R, Hall MN, Battegay EJ, Haas E. Rictor in perivascular adipose tissue controls vascular function by regulating inflammatory molecule expression. *Arterioscler Thromb Vasc Biol*. 2013;33:2105-2111.

7. Edgar R, Domrachev M, Lash AE. Gene Expression Omnibus: NCBI gene expression and hybridization array data repository. Nucleic Acids Res. 2002; 30:207-210.

8. Kreusser MM, Lehmann LH, Keranov S, Hoting MO, Oehl U, Kohlhaas M, Reil JC, Neumann K, Schneider MD, Hill JA, Dobrev D, Maack C, Maier LS, Grone HJ, Katus HA, Olson EN, Backs J. Cardiac cam kinase ii genes delta and gamma contribute to adverse remodeling but redundantly inhibit calcineurin-induced myocardial hypertrophy. *Circulation*. 2014;130:1262-1273.

9. Bordicchia M, Liu D, Amri EZ, Ailhaud G, Dessi-Fulgheri P, Zhang C, Takahashi N, Sarzani R, Collins S. Cardiac natriuretic peptides act via p38 mapk to induce the brown fat thermogenic program in mouse and human adipocytes. *J Clin Invest*. 2012;122:1022-1036.

3. Supplementary Tables and Figures:

Table S1: Summary of the hemodynamic parameters recorded in control and *Rictor*^{aP2KO} mice during the 12 hour light period, 12 hour dark period and the 12:12 hour light/dark cycle. Values represent arithmetic means ± SEM derived from 7 days of continuous measurement. n=5/6. **P*<0.05 and ***P*<0.01 versus control.

Hemo-dynamic Parameters	Control			*Rictor*^{aP2KO}		
	Light	Dark	24 hour	Light	Dark	24 hour
MAP, mm Hg	94.4±1.5	102.6±1.3	98.5±1.4	99.1±1.0	108.7±1.5*	103.9±1.1*
DAP, mm Hg	86.5±0.5	94.0±0.7	90.2±0.6	89.9±1.0*	99.4±2.0*	94.6±1.4*
SAP, mm Hg	102.6±2.7	111.4±2.5	107.0±2.6	107.4±1.9	117.2±1.7	112.3±1.7
PP, mm Hg	16.1±2.7	17.3±2.9	16.7±2.8	17.5±2.2	17.8± 2.2	17.7±2.2
HR, BPM	400.3±4.4	445.7±5.0	423.0±4.5	418.8±11.9	495.8±11.9**	457.3±10.4*

Table S2: Summary of intensity of activity and percentage of active time in control and *Rictor*^{aP2KO} mice during the 12 hour light period, 12 hour dark period and 12:12 hour light/dark cycle. Values represent arithmetic means ± SEM derived from 7 days of a continuous measurement. n=5/6. **P*<0.05, ***P*<0.01 versus control.

Locomotor Parameters	Control			*Rictor*^{aP2KO}		
	Light	Dark	24 hour	Light	Dark	24 hour
Intensity of activity, counts/min	2.0 ±0.2	6.2±0.7	4.1±0.5	4.2±1.1	10.5±2.4	7.4±1.7
Active time, %	19.6±2.3	47.1±2.3	33.4±2.2	33.5±5.6*	68.7±4.7**	51.1±5.0*

Table S3: Gene ontology analysis of micro array data revealed a significant impact of *Rictor* deletion in adipocytes on clock gene expression in PVAT from *Rictor*^{aP2KO} mice.

Process	GeneGO analysis – Pathways Maps	Total-No. of genes	Genes changed in *Rictor*^{aP2KO}	*P*-Value
1	Neurophysiological process – Circadian rhythm	47	*Bmal1, Dec1, Cry1, Rev-Erbα, Npas2*	2.051E-07
2	Cholesterol Biosynthesis	88	*Nsdhl, Cyp51A1, Fdps*	2.103E-03
3	Regulation of lipid metabolism - Regulation of lipid metabolism via LXR, NF-Y and SREBP	38	*Cyp51A1, Ldlr*	5.492E-03
4	Protein folding and maturation - Angiotensin system maturation / Rodent version	48	*Mc-cpa, Mcpt4*	8.655E-03
5	Development - TGF-beta receptor signalling	50	*Pai1, Gadd45 beta*	9.366E-03
6	Cytoskeleton remodeling	102	*Melc, Pai1*	3.588E-02

Gene ontology analysis of 68 differentially expressed genes ($P<0.05$; fold change > 1.5) was performed using GeneGo analysis program (www.genego.com). Most genes were assigned to networks involved in circadian rhythm, lipid synthesis/metabolism and cytoskeletal remodelling.

Table S4: Micro Array analysis revealed 68 genes to be differentially expressed in PVAT of *Rictor*^{aP2KO} mice compared with controls.

Probe Name	Accession	Gene Symbol	Gene Name	Log2 ratio	ratio	*P*-Value
10404389	NM_013674	*Irf4*	interferon regulatory factor 4	1.469	2.768	0.02768
10362420	NM_029726	*Trdn*	Triadin	1.257	2.39	1.12E-05
10345675	NM_008719	*Npas2*	neuronal PAS domain protein 2	1.233	2.35	0.003811
10410388	AK149411	*E430024C06Rik*	RIKEN cDNA E430024C06 gene	1.07	2.099	0.0008981
10362428	NM_029726	*Trdn*	Triadin	1.037	2.052	0.00779
10420247	NM_010779	*Mcpt4*	mast cell protease 4	0.9781	1.97	0.009402
10474972	NM_026929	*Chac1*	ChaC, cation transport regulator-like 1 (E. coli)	0.9555	1.939	0.03205
10371400	NM_007771	*Cry1*	cryptochrome 1 (photolyase-like)	0.9347	1.911	0.02016
10409278	NM_017373	*Nfil3*	nuclear factor, interleukin 3, regulated	0.8999	1.866	0.01812
10417371	NM_001024712 NM_100042149	*Gm3696;* *Gm2897*	predicted gene 3696 predicted gene 2897	0.7937	1.734	0.002434
10497451	NM_007753	*Cpa3*	carboxypeptidase A3, mast cell	0.733	1.662	0.02231
10516932	NM_144907	*Sesn2*	sestrin 2	0.7301	1.659	0.01513
10458555	NM_011898	*Spry4*	sprouty homolog 4 (Drosophila)	0.6833	1.606	0.004955
10419156	NM_053112 NM_007895 NM_007894 NM_001012766.1 NM_017388.1	*Ear10* *Ear2* *Ear1* *Ear12* *Ear3*	eosinophil-associated, ribonuclease A family, member 10 eosinophil-associated, ribonuclease A family, member 2 eosinophil-associated, ribonuclease A family, member 1 eosinophil-associated, ribonuclease A family, member 12 eosinophil-associated, ribonuclease A family, member 3	0.6264	1.544	0.03445
10556463	NM_007489	*Arntl*	aryl hydrocarbon receptor nuclear translocator-like	0.6218	1.539	0.0007209
10542885	NM_026054	*2810474O19Rik*	RIKEN cDNA 2810474O19 gene	0.6178	1.535	0.01522
10552143	NM_017394 NM_001024707	*Slc7a10* *Lrp3*	solute carrier family 7 (cationic amino acid transporter, y+ system), member 10; low density lipoprotein receptor-related protein 3	0.6174	1.534	0.02518
10436890	ENSMUST00000114029	*Gm10785*	predicted gene 10785	0.6097	1.526	0.0004848
10466304	NM_172442	*Dtx4*	deltex 4 homolog (Drosophila)	0.6033	1.519	0.002598
10461614	NM_028595	*Ms4a6c*	membrane-spanning 4-domains, subfamily A, member 6C	0.6029	1.519	0.004982
10399666	ENSMUST00000101538	*9030624G23Ri*	RIKEN cDNA 9030624G23 gene; similar to development and differentiation enhancing factor 2	0.5981	1.514	0.0001629
10407124	ENSMUST00000099179	*AI452195*	expressed sequence AI452195	0.5882	1.503	0.02528
10450784	NM_008205	*H2-M9*	histocompatibility 2, M region locus 9	0.585	1.5	0.02428

Continued table S4

Probe Name	Accession	Gene Symbol	Gene Name	Log2 ratio	ratio	*P*-Value
10349694	NM_178079	*Pm20d1*	peptidase M20 domain containing 1	-0.5872	0.6656	0.01873
10588691	NM_008317 NM_019750.3	*Hyal1* *Nat6*	hyaluronoglucosaminidase 1 N-acetyltransferase 6	-0.5907	0.664	0.03446
10527920	NM_020010	*Cyp51*	cytochrome P450, family 51	-0.5943	0.6624	0.006773
10499483	NM_134469	*Fdps*	farnesyl diphosphate synthetase	-0.597	0.6611	0.0005444
10488762	NM_009228	*Snta1*	syntrophin, acidic 1	-0.6033	0.6582	0.0006908
10399588	AJ005350	*Zfp125*	zinc finger protein 125	-0.6039	0.658	0.004791
10441774	NM_013667	*Slc22a2*	solute carrier family 22 (organic cation transporter), member 2	-0.6118	0.6544	0.02106
10480725		*BC029214*	cDNA sequence BC029214	-0.6134	0.6537	0.01623
10347224	NR_004414	*Rnu2-10*	Mus musculus U2 small nuclear RNA 10 (Rnu2), small nuclear RNA	-0.631	0.6457	0.003555
10379650	AF099974	*Slfn3*	schlafen 3	-0.631	0.6457	0.003555
10373400	NM_172259	*Myl6b*	myosin, light polypeptide 6B	-0.6414	0.6411	0.04055
10347222	NR_004414	*Rnu2-10*	Mus musculus U2 small nuclear RNA 10 (Rnu2), small nuclear RNA	-0.6423	0.6407	0.004084
10600082	NM_010941	*Nsdhl*	NAD(P) dependent steroid dehydrogenase-like	-0.6434	0.6402	0.01017
10467319	NM_011255	*Rbp4*	retinol binding protein 4, plasma	-0.6646	0.6309	0.03843
10532828	NM_029956	*Mmab*	methylmalonic aciduria (cobalamin deficiency) type B homolog (human)	-0.6656	0.6304	0.03463
10603736	NR_004414	*Rnu2*	U2 small nuclear RNA	-0.6677	0.6295	0.007948
10553354	NM_175272	*Nav2*	neuron navigator 2	-0.6863	0.6214	0.008013
10578688	NR_004414	*Rnu2*	U2 small nuclear RNA	-0.7014	0.615	0.007011
10373000	NM_026858	*Xrcc6bp1*	XRCC6 binding protein 1	-0.7098	0.6114	0.00352
10477649	NM_019811	*Acss2*	acyl-CoA synthetase short-chain family member 2	-0.7105	0.6111	0.008286
10469151	NM_172471	*Itih5*	inter-alpha (globulin) inhibitor H5	-0.7122	0.6104	0.03679
10551966	NM_001012401	*Hspb6*	heat shock protein, alpha-crystallin-related, B6	-0.717	0.6084	0.005251
10583732	NM_010700	*Ldlr*	low density lipoprotein receptor	-0.7182	0.6079	0.004846
10540472	NM_011498	*Bhlhe40*	basic helix-loop-helix family, member e40	-0.7384	0.5994	0.04434
10553092	NM_016974 NM_203280	*Dbp* *Sphk2*	D site albumin promoter binding protein sphingosine kinase 2	-0.7553	0.5924	0.0003359
10585398	NM_177350	*Gldn*	gliomedin	-0.7827	0.5813	0.04205
10381460	NR_004414	*Rnu2*	U2 small nuclear RNA	-0.7874	0.5794	0.003409
10381470	NR_004414	*Rnu2*	U2 small nuclear RNA	-0.7874	0.5794	0.003409
10381472	NR_004414	*Rnu2*	U2 small nuclear RNA	-0.7874	0.5794	0.003409
10391488	NR_004414	*Rnu2*	U2 small nuclear RNA	-0.7874	0.5794	0.003409
10381458	NR_004414	*Rnu2*	U2 small nuclear RNA	-0.8027	0.5733	0.003953
10579165	NM_007789	*Ncan*	neurocan	-0.8833	0.5421	0.02653
10417734	NM_011584	*Nr1d2*[b]	nuclear receptor subfamily 1, group D, member 2	-0.9939	0.5021	0.001567
10364149	NM_009115	*S100b*	S100 protein, beta polypeptide, neural	-1	0.4999	0.01672
10502949	ENSMUST00000083804	*snoRNA*	snoRNA	-1.067	0.4773	0.0002746
10534667	NM_008871	*Serpine1*	serine (or cysteine) peptidase inhibitor, clade E, member 1	-1.108	0.4639	0.006309
10560481	NM_008036	*Fosb*	FBJ osteosarcoma oncogene B	-1.126	0.4582	0.001421
10390691	NM_145434 NM_178060	*Nr1d1*[a] *Thra*	nuclear receptor subfamily 1, group D thyroid hormone receptor alpha	-1.255	0.419	0.0217
10364950	NM_008655	*Gadd45b*	growth arrest and DNA-damage-inducible 45 beta	-1.36	0.3897	0.009499

Micro array was performed using cDNA transcribed from RNA of PVAT from *Rictor*^{aP2KO} mice and controls and *Affymetrix Mouse Gene 1.1 ST array Strips.* Expression data were analyzed with Affymetrix Power Tools v1.10.2 (Affymetrix, Santa Clara, CA) using the RMA algorithm. Differentially expressed genes were ranked in accordance to the fold change (P<0.05) in descending order. [a] = also known as *Rev-Erbα*; [b] = also known as *Rev-Erbβ.*

Table S5: Sequences of primer pairs used for standard and quantitative real-time PCR. Primer pairs were designed using «primer blast» program (NCBI, USA) [5] and are specific to mouse cDNA. Sequences for primer pairs specific for *Anp*, *Npra*, *Nprc*, *α-Mhc* and *β-Mhc* were already described [8,9].

Gene name	Forward Primer (5'-3')	Reverse Primer (5'-3')
Anp	CAC AGA TCT GAT GGA TTT CAA GA	CCT CAT CTT CTA CCG GCA TC
Arbp	AGCTGAAGCAAAGGAAGAGTCGGA	ACTTGGTTGCTTTGGCGGGATTAG
Bhlhe40	ACG TTG AAG CAC GTG AAA GC	CTT CCC GAC AAA TCA CCA GC
Bmal1	ACT ACA GTG GCC CTT TG CAT	GCC CAA ATT CCC ACA TCT GAA G
Bnp1	GTC TGG CCG GAC ACT CAG	TGC ACT GGT GTC TTC AAC AAC
Clock	TTA GAT CAC AGG GCA CCA CC	AGT GCT CGT GAC ATT TTG CC
Cnp	GAC ACC ACC GAA GGT CCC G	CCT GGA GTC TTG TCA CCC TTT T
Cre	GCG GTC TGG CAG TAA AAA CTA TC	ACC CGG CTG CTC TTA CTT CT
Cry 1	ATG TCC CGA GTT GTA GCA GC	TGA GAG CAA TTT CCA CCG CT
Cry 2	AGC TGA TGT GTT CCC AAG GCT	CAT AAT GGC TGC ATC CCG TT
Cyclophelin B	GGT GGA GAG CAC CAA GAC AGA	GCC GGA GTC GAC AAT GAT G
Dbp	GGA ACT GAA GCC TCA ACC AAT C	CTC CGG CTC CAG TAC TTC TCA
Gapdh	AAA TGG TGA AGG TCG GTG TG	GTT GAA TTT GCC GTG AGT GG
Nfil3	GAG CAG AAC CAC GAT AAC CCA T	TAC AGA CCG GAT GGA GGA GAC
Npas2	AGA GGC AGC TTG AAC CCA AA	GAG GGG CTA GGC ACA TTG TT
Npra	CGA AGA CAA GTG CAT CCT GAG	TGG AGA CAC AGT CAA CAC AGC
Nprb	ACC GGT CAC TTC AAG GGA AA	GGC TCC GAT GAA GCG AGT AA
Nprc	AGC TGG CTA CAG CAA GAA GG	CGG CGA TAC CTT CAA ATG TC
Per1	CCA GAT TGG TGG AGG TTA CTG AGT	GCG AGA GTC TTC TTG GAG CAG TAG
Per2	AGA ACG CGG ATA TGT TTG CTG	ATC TAA GCC GCT GCA CAC ACT
Rev-Erb-α	TGT CTA GAG ATG CTG TGC GTT T	AGG CTG CTC AGT TGG TTG TT
Rictor (PCR)	TTA TTA ACT GTG TGT GGG TTG	CGT CTT AGT GTT GCT GTC TAG
Rictor (qRT-PCR)	TGC GAT ATT GGC CAT AGT GA	ACC CGG CTG CTC TTA CTT CT
Rorα	GCT TCT AAA AGC AGG CTC GC	GGG ACT TGA AGA CAT CGG GG
Tbp	GAG TTG CTT GCT CTG TGC TG	CTG GCT TGT GTG GGA AAG AT
α-Mhc	CGC ATC AAG GAG CTC ACC	CCT GCA GCC GCA TTA AGT
β-Actin	CGT GCG TGA CAT CAA AGA GA	CCC AAG AAG GAA GGC TGG A
β-Mhc	CGC ATC AAG GAG CTC ACC	CTG CAG CCG CAG TAG GTT

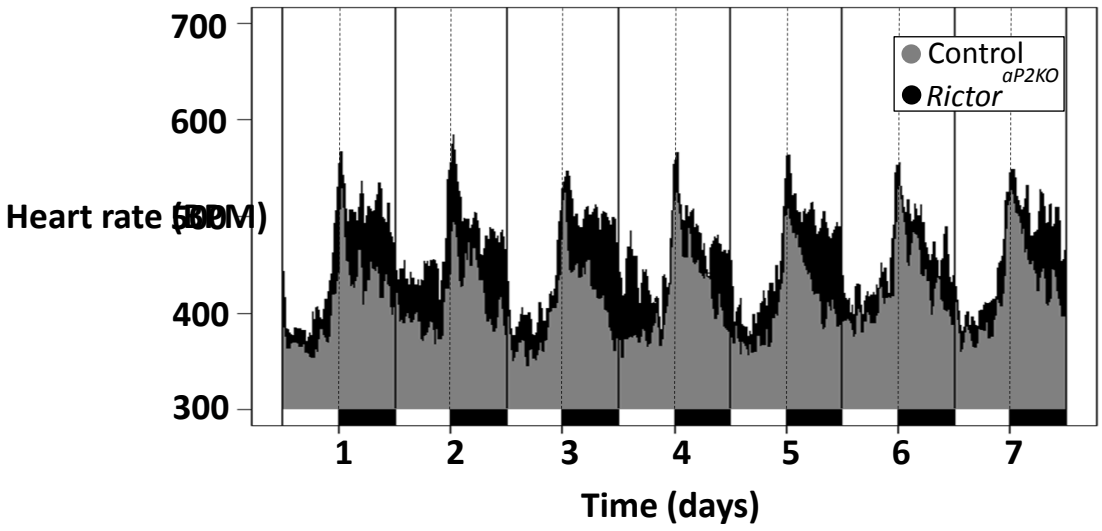

Figure S1: Heart rate is increased and its physiological decline during the dark period nearly absent in *Rictor*^{aP2KO} mice. Heart rate (HR) was recorded over a period of 7 consecutive days in *Rictor*^{aP2KO} and control mice (n=5/6) kept in a constant 12:12 hour light/ dark cycle (light on: 7 am/ ZT 0; light off: 7 pm/ ZT 12). Diurnal fluctuations of HR are represented as one hour running median. Black bars at the bottom denote the 12 hour dark period.

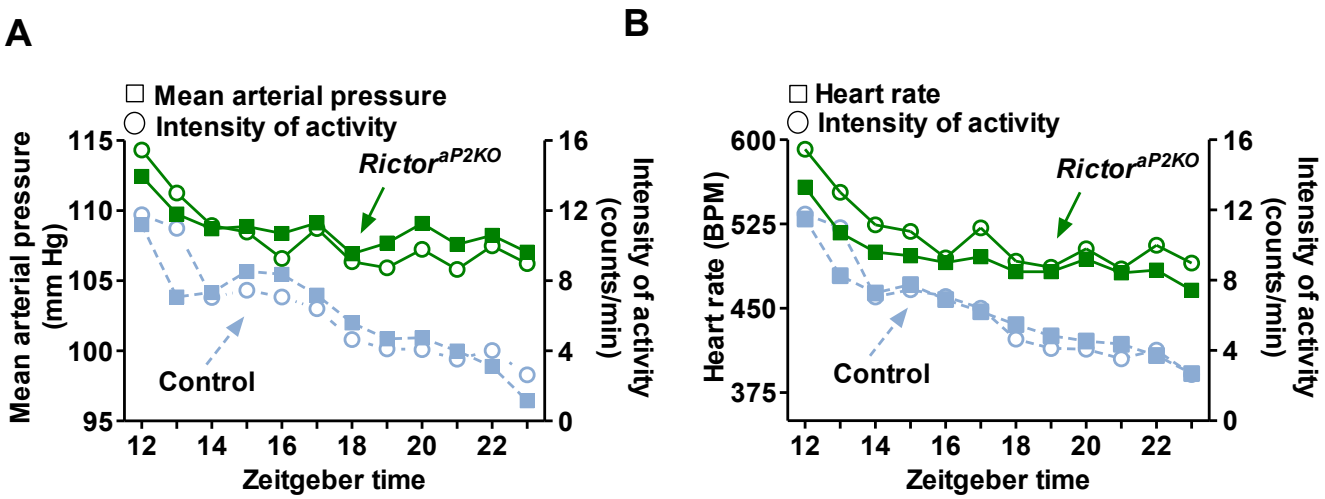

Figure S2: Time courses of mean arterial pressure, heart rate and locomotor activity display similar patterns and are less steep in *Rictor*^{aP2KO} mice during the dark period. Intensity of activity, mean arterial pressure (MAP, **A**) and heart rate (HR, **B**) were recorded over a period of 7 consecutive days in *Rictor*^{aP2KO} and control mice (n=5/6) kept in constant 12:12 hour light/ dark cycles. Hourly means of the measured parameters at the indicated time points are represented.

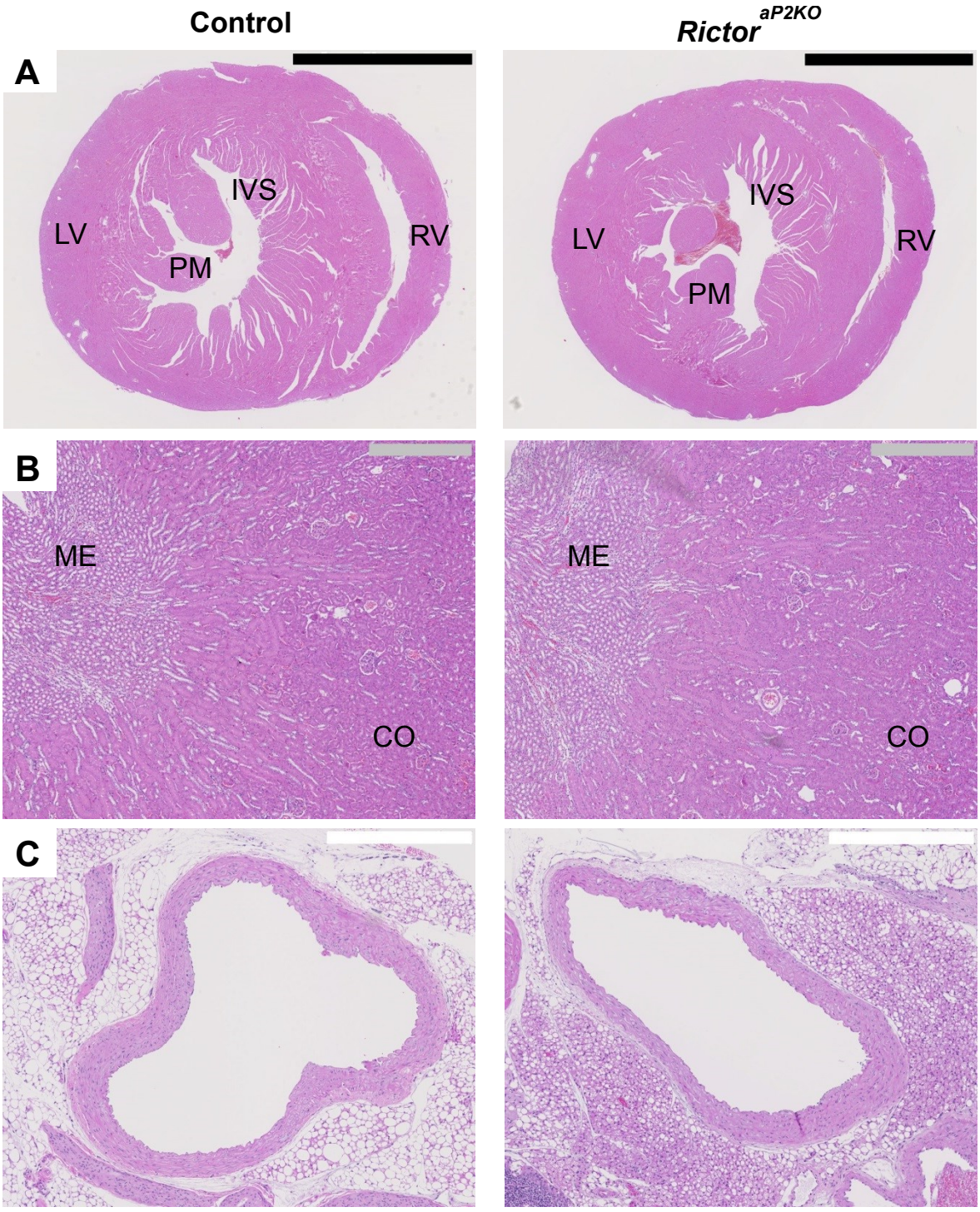

Figure S3: *aP2*/CRE-driven deletion of *Rictor* affects cell density of aortic PVAT, while no differences in the heart and kidney are noted. Representative cross-sections stained with haematoxylin/eosin of **(A)** the heart, **(B)** the kidney, and **(C)** the aortic arch with PVAT are shown. Heart sections in A were performed at the level of the papillary muscles. Black bar: 2.5 mm. Grey bar: 500 µm. White bar: 500 µm. CO (cortex), ME (medulla), IVS (interventricular septum), LV (left ventricle), PM (papillary muscles), RV (right ventricle).

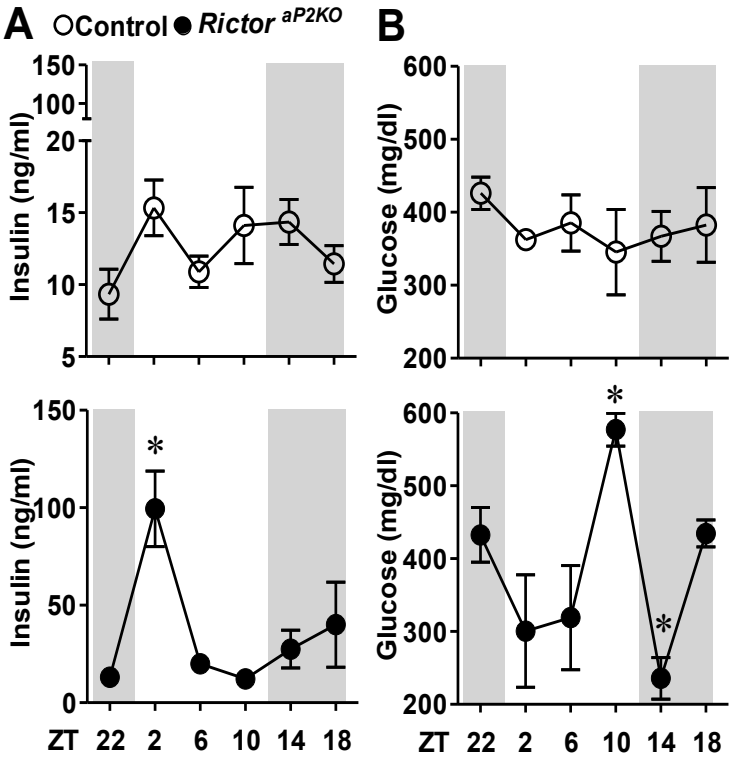

Figure S4: Strong variations in glucose and insulin plasma levels during a 24 hour cycle in *Rictor*^{aP2KO} mice. (A) Insulin and **(B)** glucose concentrations were determined in blood plasma using BioPlex assay and UniCel DxC 800 System, respectively. Grey shaded areas represent the 12 hour dark period. ZT: Zeitgeber time. Values represent mean ± SEM. n=3. *P<0.05 versus control.

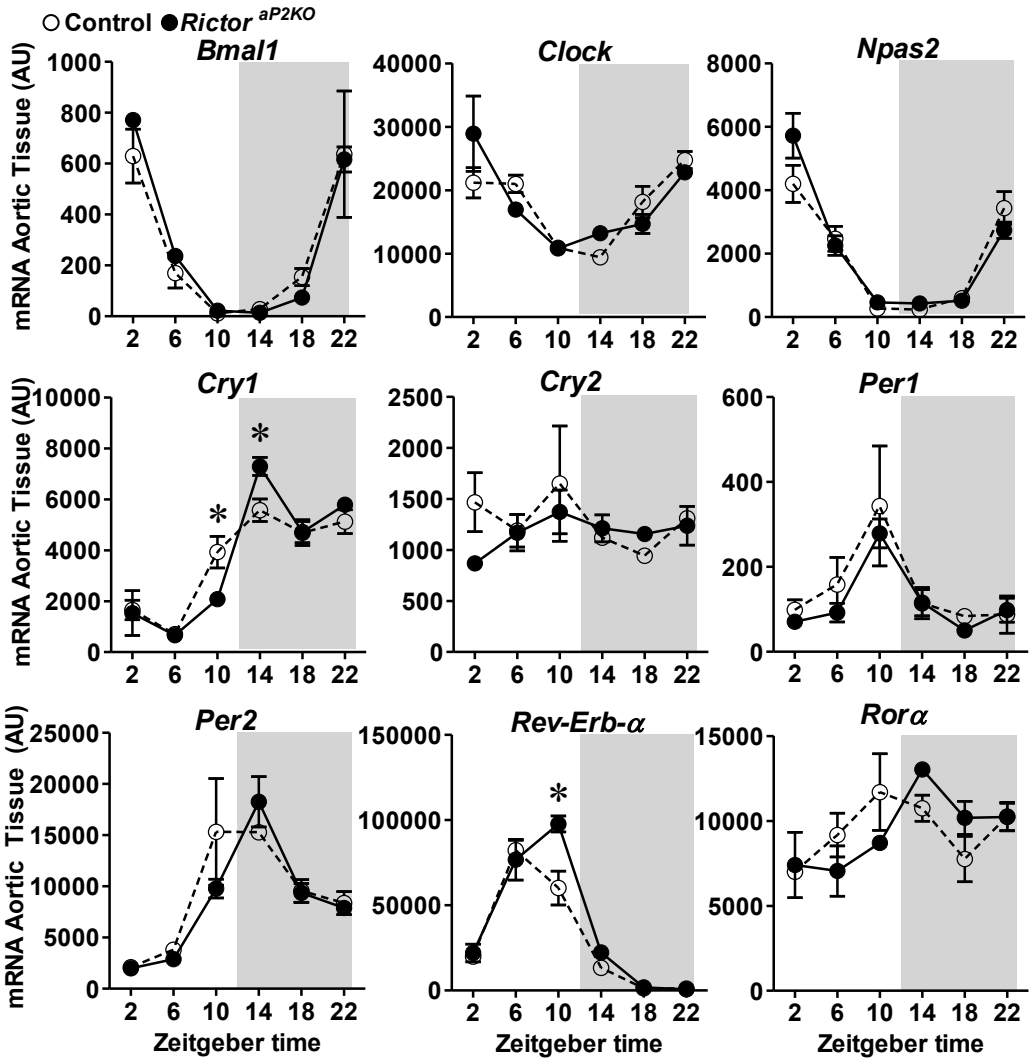

Figure S5: Steady state mRNA expression levels of core clock genes are similar in aortic tissue from control and *Rictor*^{aP2KO} mice. mRNA expression levels of core clock genes in aortic tissue were determined using qRT-PCR. Grey shaded areas represent the dark period. Values are expressed in arbitrary units (AU). n=3 per group and time point**.** **P*<0.05 versus control.

Hypertension
Journal of the American Heart Association

Deletion of *Rictor* in Brain and Fat Alters Peripheral Clock Gene Expression and Increases Blood Pressure

Katja Drägert, Indranil Bhattacharya, Giovanni Pellegrini, Petra Seebeck, Abdelhalim Azzi, Steven A. Brown, Stavroula Georgiopoulou, Ulrike Held, Przemyslaw Blyszczuk, Margarete Arras, Rok Humar, Michael N. Hall, Edouard Battegay and Elvira Haas

Hypertension. published online June 22, 2015;
Hypertension is published by the American Heart Association, 7272 Greenville Avenue, Dallas, TX 75231

Print ISSN: 0194-911X. Online ISSN: 1524-4563